Universitätsklinikum Hamburg-Eppendorf

Institut für Osteologie und Biomechanik
Zentrum für experimentelle Medizin
Universitätsklinikum Hamburg-Eppendorf

Direktor: Prof. Dr. med. Michael Amling

The comparative analysis of Wnt1 overexpression underlines a differential effect of Wnt on the ectopic mineralization of the tooth pulp

Dissertation

zur Erlangung des Grades eines Doktors der Medizin /Zahnmedizin
an der Medizinischen Fakultät der Universität Hamburg.

vorgelegt von:

Nannan Liao
aus Hebei, China

Hamburg 2020

Angenommen von der
Medizinischen Fakultät der Universität Hamburg am: 05.06.2020

Veröffentlicht mit Genehmigung der
Medizinischen Fakultät der Universität Hamburg.

Prüfungsausschuss, der/die Vorsitzende: Prof.Dr.Thorsten Schinke

Prüfungsausschuss, zweite/r Gutachter/in: PD Dr. Sabine Windhorst

Table of Contents

1. Introduction

1.1 Task

Bone is a dynamic mineralized tissue, which is constantly renewed. When bone homeostasis (the balance of deposition by osteoblasts and resorption by osteoclasts) is disrupted, bone is negatively (osteoporosis or osteogenesis imperfecta) or positively (sclerosteosis and Van Buchem disease) affected. Since there is an increasing number of reports about diseases associated with mutations of Wnt signaling components (Gong et al. (2001); Brunkow et al. (2001); Toomes et al. (2004)), it is gradually confirmed that Wnt signaling is important in the regulation of bone homeostasis. Activation of the Wnt signaling pathway leads to an increase in bone mass and strength, whereas inhibition leads to a decrease. The Wnt1 gene is the first Wnt gene that was identified by Nusse and Varmus in 1982 (Nusse and Varmus (1982)). Initially established as a proto-oncogene, it was demonstrated 30 years later that Wnt1 also affects bone metabolism. In fact, Wnt1 mutations were found to cause either early-onset osteoporosis or osteogenesis imperfecta (Pyott et al. (2013a)). Moreover, our group showed that an osteoblast-specific induction of Wnt1 expression causes a rapid increase of bone formation (Luther et al. (2018)).

As another mineralized tissue in the human body, the tooth performs important physiological functions in daily life such as mastication and speech. During tooth development, components of Wnt signaling are detected. Whereas Wnt3, Wnt4, and Wnt6 are expressed in the epithelium (Sarkar and Sharpe (1999); Wang et al. (2014)), Wnt5a is expressed in the mesenchyme and dental papilla (Wang et al. (2014)). However, it is unclear what the impact of Wnt1 is and what kind of Wnt signaling pathway is relevant for tooth development.

The aim of this work was therefore to clarify the influence of Wnt1 on tooth development using a genetically modified mouse model with inducible Wnt1-overexpression.

1.2 Anatomical basic

1.2.1 Murine dental anatomy

Although the development of dentition is considered to be highly conserved between humans and mice, the murine dentition is reduced as compared to that of humans. The mouse has only 16 teeth - one continuously growing incisor and three molars in each quadrant separated by a large diastema (Figure 1.1) (Luckett (1985)). Tooth eruption is also simplified as mice have only one set of teeth (Peterková et al. (1995); Keränen et al. (1999)).

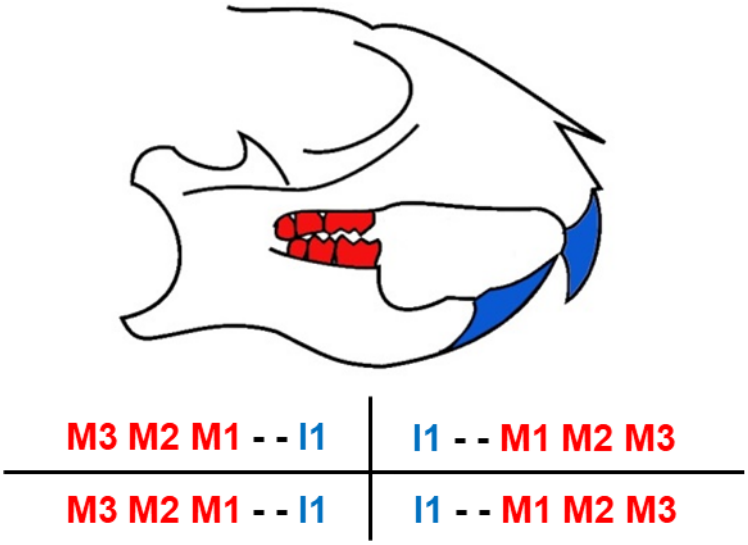

Figure 1.1 Schematic right view of the mouse skull with related tooth scheme. The incisors are colored blue, the molars colored red.

However, mice and human teeth share the same basic morphology. The upper third of the teeth consists of a crown facing towards the oral cavity and the lower two-thirds of a root anchoring through periodontal fibers in the alveolar bone. The teeth are composed of three specialized calcified tissues: dentin, enamel and cementum. Dentin is secreted by odontoblasts and constitutes the main part of the crown and the root. The crown is covered by enamel, the hardest substance of the body, and the root is covered by cementum. The junction between the enamel and the cementum layer defines the anatomical boundary between the crown and the root. The cementum provides attachment for periodontal fibers anchoring the tooth in the alveolar bone. The pulp, a

soft tissue consisting of nerves, fibers and blood vessels, compromises the central part of the tooth (Figure 1.2).

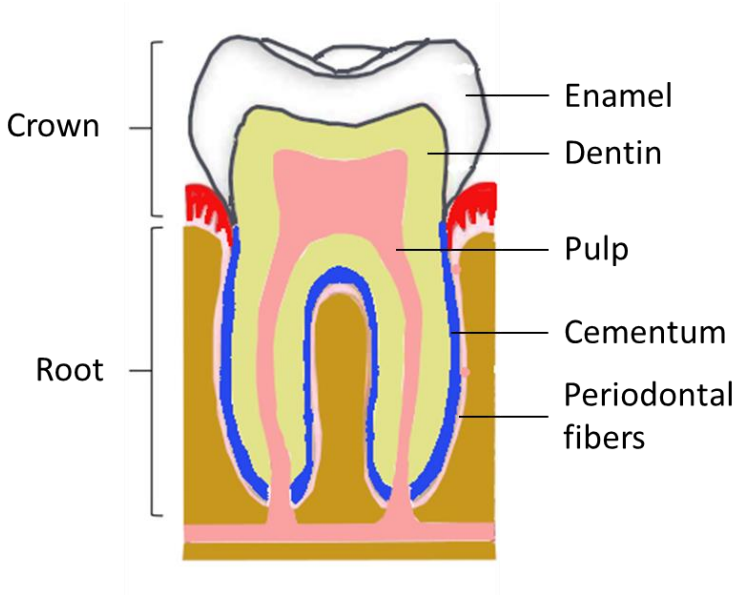

Figure 1.2 Schematic diagram of tooth structure. The tooth has two parts - the crown and the root. Enamel, the hardest substance in the body, covers the dentin in the crown and cementum covers the dentin in the root surface. Pulp is located in the center of the tooth.

1.2.2 Murine tooth development

More than a hundred years ago, tooth development was described in detail for many animals and also for humans. Tooth development initiates within the oral epithelium, which thickens at embryonic day 11.5 (E11.5) (Jheon et al. (2013)) and eventually becomes the dental lamina. The thickened oral epithelium is the result of a series of reciprocal interactions between epithelial and mesenchymal cells (Thesleff and Sharpe (1997)). Subsequently, the tooth bud (E12.5-E13.5) continues to proliferate, and the tooth germ progresses through the cap (E14.5-E15.5) and bell stage (E16.5-E20). Finally, the tooth crown is forming. The inner enamel epithelium differentiates into ameloblasts at the late bell stage, and the outer layer of the dental mesenchyme differentiates into odontoblasts at the same stage. Ameloblasts secret enamel till tooth eruption occurs and odontoblasts secret dentin throughout life. After crown formation

dentinoblasts migrate apically to form the tooth root. This process is guided by the Hertwig's epithelial root sheath (HERS), a double-layered epithelial structure that extends from the apical region of the enamel organ. As soon as root formation is initiated, the HERS degenerates and cementoblasts are secreting cementum on the dentin surface (Schour and Massler (1940)). (Figure 1.3) (Thesleff (2014))

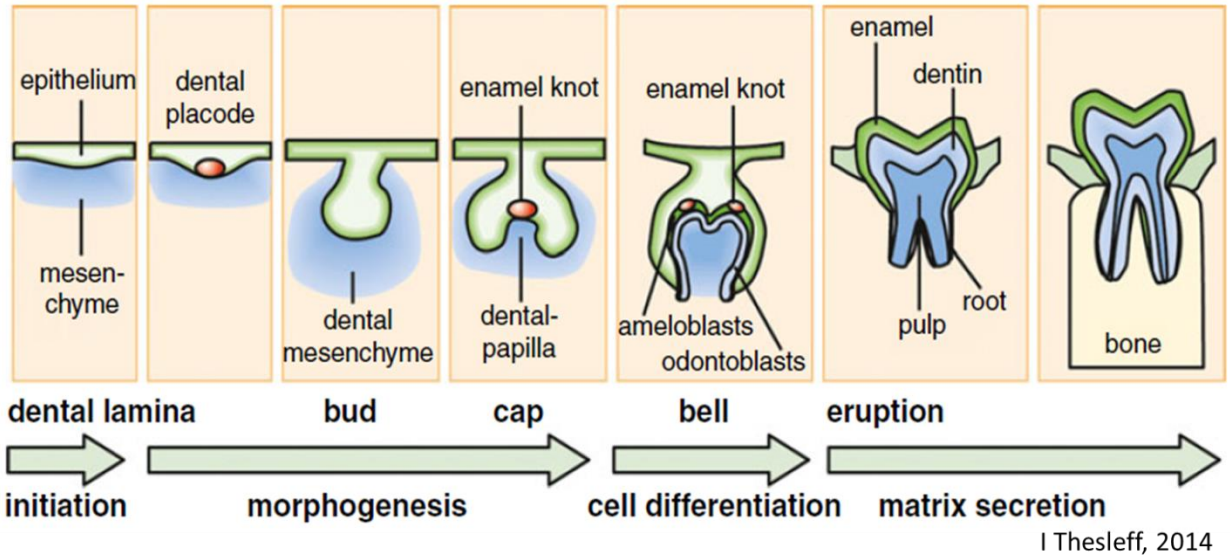

Figure 1.3 The process of tooth development. The tooth development starts from the thickening of the epithelium which is followed by condensation of the mesenchymal cells. The tooth crown forms through stages defined by the shape of the epithelium (bud, cap, bell) followed by the development of the root. (Thesleff (2014))

1.3 Signaling networks that regulate tooth development

Research about the molecular mechanisms of tooth development started in the late 1980s. Many signaling pathways work together to coordinate tooth development, and this section summarizes some of the major pathways.

1.3.1 FGF signaling

The Fibroblast Growth Factors (FGFs) are comprised of twenty-three secreted proteins that interact with four signaling tyrosine kinase FGF receptors (FGFRs). Multiple FGF family members mediate a wide variety of tooth development processes, i.e. the

formation of dental tissue, regulating the size and shape of the tooth, as well as the development of the stem cell in mouse incisor. Epithelial Fgf8, Fgf9, Fgf10 and Fgf17 expression are detected during the initiation of tooth development (Porntaveetus et al. (2011); Kettunen and Thesleff (1998); Yokohama-Tamaki et al. (2006)). A recent study has revealed that the expression of Fgf8 and Fgf17 are important for prospective molar positioning (Porntaveetus et al. (2011); Prochazka et al. (2015)) and are also critical in determining the tooth type (Neubüser et al. (1997); Tucker et al. (1999)). During the phases from the epithelial thickening to the dental lamina, Fgf10 expression decreases in the epithelium, whereas the expression of Fgf8 and Fgf9 is maintained (De Moerlooze et al. (2000); Hosokawa et al. (2009)). At the bud stage, Fgf8 is expressed in the epithelium in order to regulate the transcription factor PITTX2 (St Amand et al. (2000)), which is important for tooth formation. From the cap stage to the bell stage, FGF signaling is important in the differentiation of ameloblasts and odontoblasts. Fgfr1 and Fgfr2IIIb are expressed in the ameloblasts (Takamori et al. (2008)). In mesenchymal cells, the expression of Fgf3 and Fgf10 was found to negatively regulate the differentiation of dental papilla cells into odontoblasts (Kettunen et al. (2000); Kyrylkova et al. (2012)).

1.3.2 BMP/Tgf-β signaling

Bone morphogenetic proteins (BMPs) which belong to the TGF-β superfamily, play pivotal roles at multiple stages during tooth development (Jernvall and Thesleff (2000)). During the main stages of tooth development, several BMP genes, including BMP-2, BMP-3, BMP-4 and BMP-7, are expressed in either the epithelial or mesenchymal components (Nie and Sage (2009)). In particular, BMP-4 is an important gene mediating the BMP/TGF-β signaling throughout the main stages of tooth formation: initiation, bud, cap and bell (Vainio et al. (1993)). At the initiation stage of tooth development, BMP-4 is expressed in the epithelium and induces MSX homeobox 1 gene expression, which is crucial in early tooth development (Maas and Bei (1997)). Later, while the epithelium thickens at the dental lamina stage, BMP-4 expression is detected in both the epithelium and the mesenchyme. Mesenchymal BMP-4 expression negatively regulates Pax9, which plays a critical role in tooth development (Neubüser et al. (1997)). During the following bud stage, BMP-4 binds to its receptor and reduces the expression of Ldf1,

which is an important transcription factor in canonical Wnt/β-Catenin signaling (Kratochwil et al. (1996)). Subsequently, at the cap stage, BMP-4 is intensively expressed in the enamel knot, which controls the tooth type and the shape of the crown (Jernvall et al. (1998); Vaahtokari et al. (1996); Dassule and McMahon (1998)).

1.3.3 SHH signaling

Sonic hedgehog (Shh) signaling plays a critical role in multiple tooth developmental processes. Shh secretion starts at the dental lamina stage (Biggs and Mikkola (2014); Pispa and Thesleff (2003)). Shh expression is inhibited by Wnt7b in the non-odontogenic epithelium domains that defines where the teeth are forming (Sarkar et al. (2000)). Recent studies revealed that Shh signaling acts synergistically with Fgf signaling and induces the proliferation of the epithelium during early stages of tooth development (Li et al. (2016)). Afterwards, Shh expression is upregulated in the enamel knot, and coordinates with Fgf-3, -4 and -9; BMP-2, -4 and -7; Wnt10a and 10b to define the tooth shape (Vaahtokari et al. (1996); Ahn et al. (2010); Klein et al. (2006); Pummila et al. (2007); Murashima-Suginami et al. (2008)). S.W. Cho proposed a Shh–Wise–Wnt feedback model in the enamel knot to regulate dental morphogenesis (Cho et al. (2011)). At the bell stage, Shh is intensively expressed in the inner enamel epithelium (IEE) to mediate cytodifferentiation in the tooth germ (Gritli-Linde et al. (2002)).

1.3.4 WNT signaling

1.3.4.1 Wnt signaling and their components

After Wnt1 (Int-1) was identified as the first member of the Wnt family in a mouse mammary tumor study (Nusse and Varmus (1982)), more and more Wnt signaling components were detected to play essential roles in the development and tissue homeostasis of multicellular organisms (Logan and Nusse (2004)). In mammals, there are 19 Wnt ligands and two distinct Wnt signaling pathways - the canonical pathway and the noncanonical pathway.

The Wnt/β-catenin pathway is initiated by binding of Wnt ligands to receptors of the seven-transmembrane domain- spanning Frizzled family (Logan and Nusse (2004)) and the co-receptors lipoprotein receptor-related proteins (LRP) 5/6 (He et al. (2004)). This causes recruitment of Dishevelled (DVL) proteins and Axin complexes to the intracellular

site of the Frizzled and the LRP5/6 receptors, thereby preventing phosphorylation and proteasomal degradation of β-catenin. Stabilization of β-catenin results in its translocation to the nucleus. Translocated β-catenin displaces the groucho proteins and associates with T-cell factor/lymphoid enhancer-binding factor (TCF/LEF) transcription factors to control Wnt target genes (i.g. CyclinD, c-myc, Axin2 et al.) transcription (Arce et al. (2006)). The scaffold protein Axin and APC are phosphorylated by Casein kinase 1 (CK1) and Glycogen Synthase Kinase 3 Beta (GSK3β), which can enhance the phosphorylation and degradation of β-catenin. Therefore, Axin is a negative regulator of the canonical Wnt signaling pathway (Huang and He (2008);Kimelman and Xu (2006)). (Figure 1.4)

Noncanonical Wnt signaling is defined as a signaling pathway that is independent of β-catenin transduction. There are several noncanonical Wnt signaling pathways. Here we introduce only the Wnt/PCP signaling pathway, which is the best characterized noncanonical Wnt signaling pathway. Wnt/PCP signaling plays a critical role in polarity of tissues and mesenchymal cells. It is initiated by binding of Wnt ligands to the Frizzled-receptors. This leads to the recruitment of Dvl to the Frizzled and activates downstream regulation of actin cytoskeleton/cell adhesion. For instance, the Dvl binds Dishevelled-associated activator of morphogenesis 1 (DAAM1) to activate the small G-protein Rho, which leads to Rock kinase activation and MRLC phosphorylation; Dvl forms a complex with Rac1 to activate JNK kinase, which may phosphorylate CapZIP/Dub (Schlessinger et al. (2009)). (Figure 1.4)

In addition, several secreted Wnt antagonists were identified: secreted frizzled related proteins (SFRPs), Wnt inhibitory factor-1 (WIF-1), Dickkopf (DKK), Sclerostin (SOST) and Wise, all of them with slightly different mode of action. SFRPs and WIF-1 bind to the Wnt ligand, which interferes Frizzled binding and causes suppression of Wnt signaling (Bovolenta et al. (2008)). In contrast, SOST inhibits Wnt signaling through binding to LRP5/6 (van Amerongen and Nusse (2009)). DKK coordinates with LRP5/6 and Kremen resulting in suppression of the canonical Wnt signaling pathway (Nakamura et al. (2008)) and Wise also was reported to inhibit Wnt signaling in interaction with LRP6 (Lintern et al. (2009)).

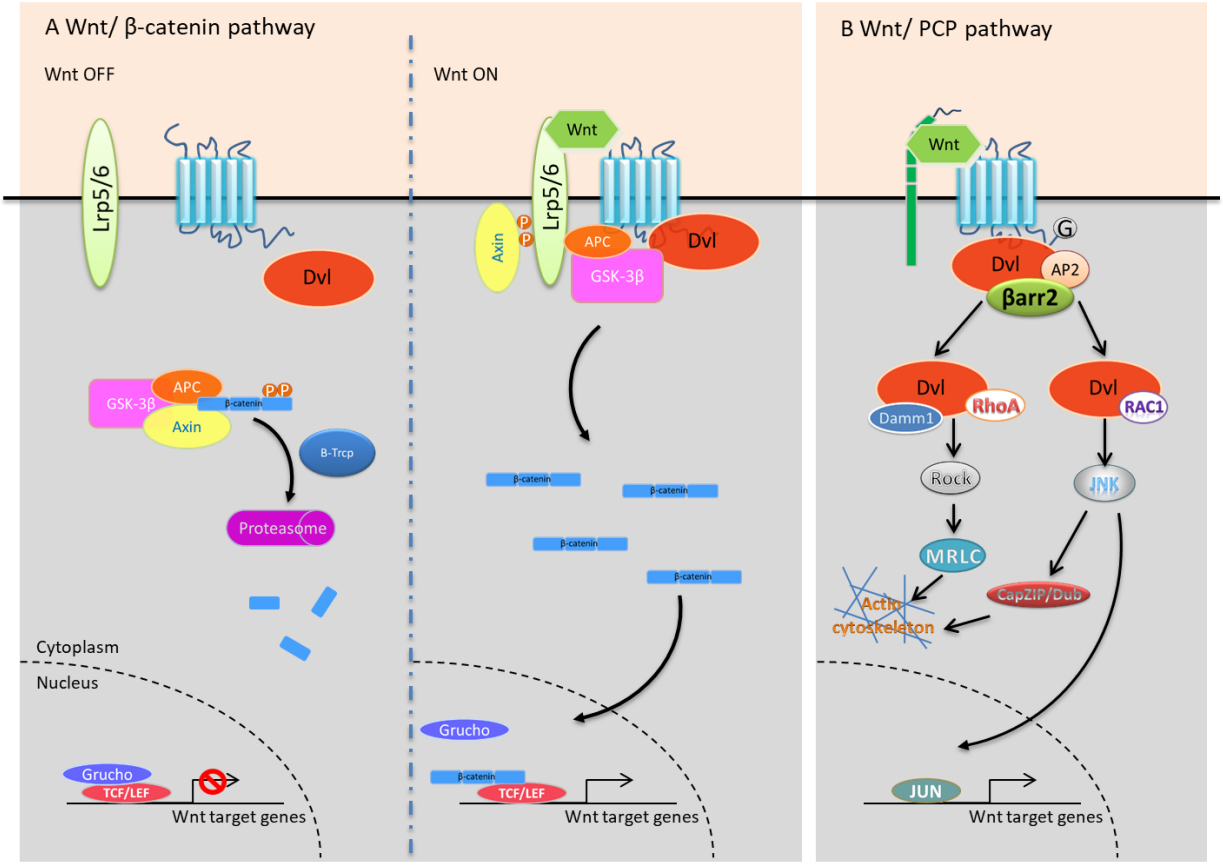

Figure 1.4 Wnt signaling network. A) Wnt OFF: In the absence of Wnt, cytoplasmic β-catenin is bound and phosphorylated by the destruction complex which is including Axin, APC and GSK-3β. Then the phosphorylated β-catenin is ubiquitinated by β-TrCP and degraded by proteasome. Wnt ON: Upon Wnt binding to the canonical Fzd and co-receptor Lrp5/6, the destruction complex falls apart and Dvl, Axin, APC and GSK-3β are recruited to the plasma membrane, thus β-catenin is stabilized. B-catenin subsequently translocates to the nucleus and binds with TCF/LEF to activate Wnt responsive genes. B) In the Wnt/PCP pathway, Wnt5a and Wnt11 binding with Fzd may activate trimeric G proteins and Dvl complexes. Multiple pathways downstream of Dvl regulate cytoskeleton / cell adhesion of actin. The Dvl-Daam1-RhoA complex activates RhoA, resulting in Rock kinase activation and MRLC phosphorylation. The Dv1-Rac1 complex activates JNK kinase, which may phosphorylate CapZIP / Dub.

1.3.4.2 Wnt signaling pathway in tooth development

During tooth development, the Wnt signaling pathway plays essential roles in cell differentiation, proliferation and migration. At different phases of tooth development,

many Wnt signaling compounds were detected, such as the ligands Wnt2, 3, 4, 5, 6, 7 and 10, the Wnt signaling receptors/coreceptor Fz6 and LRP 5/6, as well as Wnt antagonists including DDK, Sfrp1, Wise, et al (Sarkar and Sharpe (1999); Wang et al. (2014)).

Among the multiple Wnt genes expressed during the tooth development, some were determined to be more important, such as Wnt10a and Wnt10b. More specifically, Wnt10a and Wnt10b were both detected in the molar and incisor dental epithelium at the initiation and bud stages and in the enamel knot at the cap stage of tooth development. Wnt10b was also observed in inner enamel epithelium at the bell stage (Dassule and McMahon (1998); Sarkar and Sharpe (1999)). It is clear that the spatial and temporal distribution of Wnt10a expression is essential for the induction of dentin sialophosphoprotein (Dspp) expression (Yamashiro et al. (2007)). These data suggest that Wnt10a plays an important role in tooth root formation.

During tooth development, another important Wnt gene is Wnt5a. Wnt5a which is a representative protein of the noncanonical Wnts actives both the canonical Wnt signaling by binding to Fz5 and the noncanonical Wnt signaling by binding to ROR2. Wnt5a can be detected in dental mesenchyme at initiation and bud stages, and in the dental papilla and dental sac at cap and bell stages (Sarkar and Sharpe (1999)). Here, Wnt5a/Fz5 signaling mediates axis induction ("Entrez Gene: WNT5A wingless-type MMTV integration site family, member 5A"), and Wnt5a/ROR2 signaling mediates cell differentiation, proliferation, polarity and apoptosis (Gordon and Nusse (2006); Mikels et al. (2009)). For tooth development, Wnt5a promotes the differentiation of human dental papilla cells (hDPCs) (Peng et al. (2010)). The analysis of Wnt5a-deficient mice suggested that Wnt5a regulates odontoblast differentiation during odontogenesis (Lin et al. (2011)). When siRNA was used to kockdown the Wnt5a expression in SVF4 cells (dental papilla cell line), the Wnt3a-induced ALP expression was upregulated, indicating that Wnt5a has a negative function in canonical Wnt signaling at early dental follicle cell differentiation (Sakisaka et al. (2015)).

Wnt3 can be detected in several tooth development phases including in oral epithelium at the initiation stage, in enamel knot at the cap stage and in inner enamel epithelium at the bell stage. Rat dental pulp repair experiments show that liposomal delivery of Wnt3a

can protect dental pulp cells from cell death and stimulate the proliferation of undifferentiated dental pulp cells, thereby improving the healing of rat dental pulp (Hunter et al. (2015)). Wnt3a expression was observed in HERS cells during mouse tooth root formation. Wnt3a induced ALP, Runx2 and Osterix expression in immortalized murine dental follicle cells suggesting that Wnt3a plays a crucial role in tooth root formation (Nemoto et al. (2016)).

Moreover, other compounds of Wnt signaling pathway are also important for tooth development. During the bud stage, Dkk1 is continuously expressed in the dental epithelial and mesenchymal cells, where it arrest the tooth development (Bei and Maas (1998); Liu et al. (2008)). Subsequently, Dkk1 expression is up-regulated in pro-odontoblasts and secretory odontoblasts (Fjeld et al. (2005)). Axin2, as a direct target of the Wnt signaling pathway, is expressed in developing odontoblasts and dental pulp cells (Lohi et al. (2010)). The expression of β-catenin and Lef1 in the dental epithelium at the bud stage is also critical for tooth development. More specifically, inactive β-catenin and Lef1 repress PITX2 expression and cause an arrest of tooth development (Hjalt et al. (2000); van Genderen et al. (1994)).

There is also evidence for a Wnt signaling pathway crosstalk with FGF and Shh signals. At the bud stage, Fgf4 expression is detected in the epithelium, where it may function as a transcriptional target gene of Wnt signaling (van Genderen et al. (1994); Kratochwil et al. (2002)). At the cap stage, Wnt and Shh signaling form a Shh-Wise-Wnt feedback loop, which is responsible for tooth pattern formation (Cho et al. (2011)). Collectively, these observations indicate that the Wnt signaling pathway plays crucial roles in tooth development.

1.3.4.3 Wnt1 influences on murine bones and teeth

Wnt1 is the first Wnt family member reported by Nusse and Varmus in 1982 (Nusse and Varmus (1982)). Wnt1 was first identified as a gene that is activated by the integration of mouse mammary tumor virus in virally induced breast tumors, and was subsequently detected as a homologous gene to the fly Wingless gene, which controls segment polarity during larval development in Drosophila melanogaster (Nüsslein-Volhard et al. (1980); Rijsewijk et al. (1987)). In 2013, the Wnt1 mutations were reported to cause both

early-onset osteoporosis and osteogenesis imperfecta (OI) in the bone though the Wnt signaling pathway (Laine et al. (2013)). Since then, a variety of Wnt1 mutations were reported to induce skeletal morbidity (Pyott et al. (2013b); Keupp et al. (2013); Faqeih et al. (2013); Stephen et al. (2015); Aldinger et al. (2016); Liu et al. (2016)).

We therefore studied the influence of murine Wnt1 on bone formation and remodeling. We analyzed histological sections of undecalcified spines and tibiae of transgenic mice with inducible Wnt1 over-expression (Luther et al. (2018)). The trabecular bone volume and cortical thickness were increased in 6-week-old mice 3 weeks after transgene induction (Figure 1.5). Similar findings were obatined in 12-week-old male mice (9 weeks after induction of the transgene). The cortical thickness increase, confirmed by µCT images and quantitative results shows that Wnt1 has a bone-anabolic function in both bone compartments (Luther et al. (2018)).

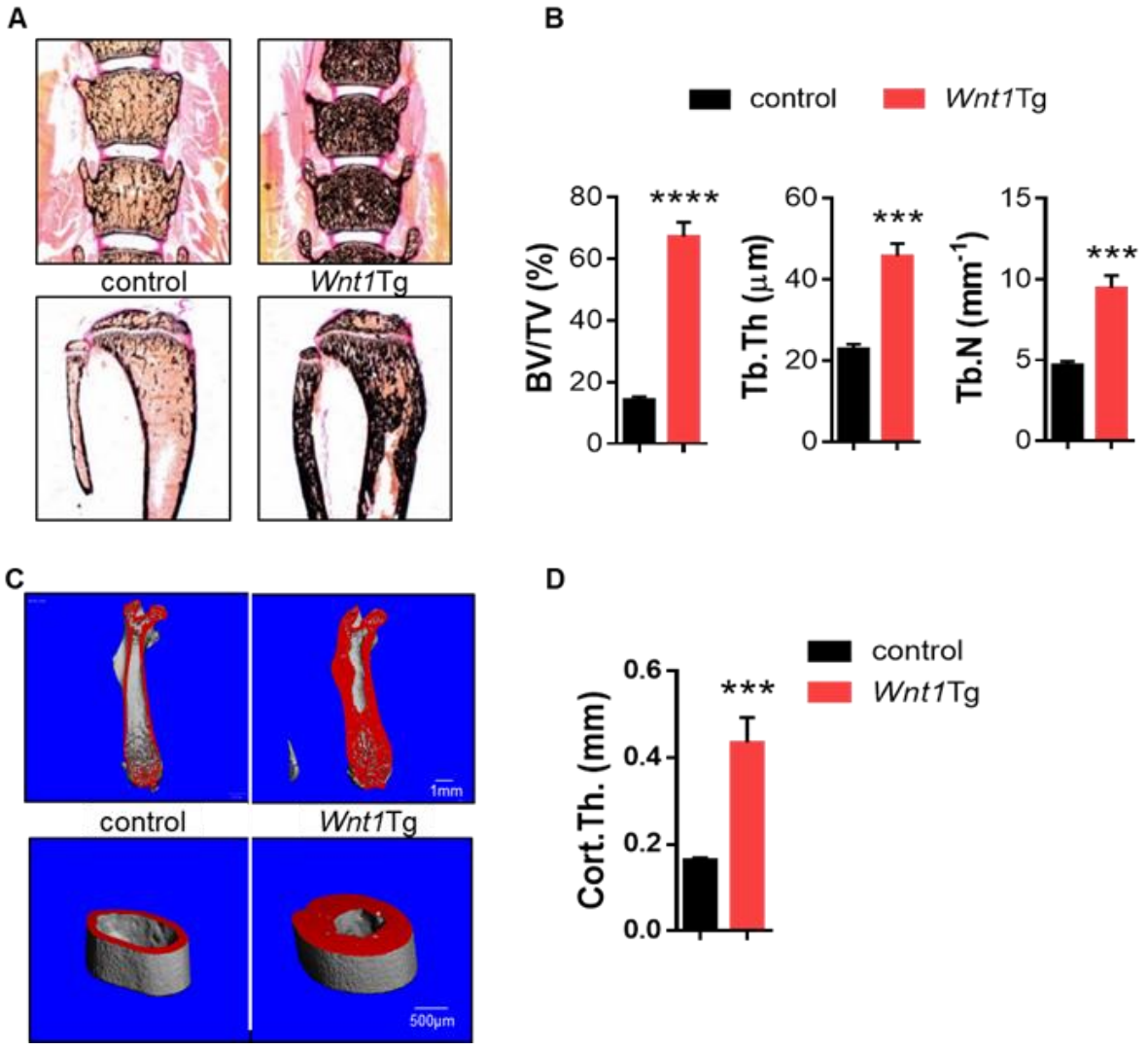

Figure 1.5 Wnt1 induction caused high bone mass in growing mice. A) Von Kossa staining of vertebrae and tibiae of 6-week-old control and *Wnt1*Tg male mice with DOX free diet for 3 weeks. B) Histomorphometric quantification of trabecular bone parameters (BV/TV = bone volume per tissue volume, Tb.Th = trabecular thickness and Tb.N = trabecular number). C) µCT imaging of the femora from 12-week-old male control and *Wnt1*-transgenic mice (9 weeks after induction of the transgene). D) µCT quantification of cortical bone parameters. (Cort.Th = cortical thickness). n⩾4. Data are the means ± SEM. ****P < 0.0001; ***P < 0.001.

We further analyzed the teeth and the alveolar bone in these mice. µCT imaging showed that Wnt1 induction alters the structure of both, alveolar bone and teeth (Figure 1.6). By quantification we confirmed that the visible root area was decreased by Wnt1 induction, whereas the distance between the cementum enamel junction and the alveolar bone

crest was significantly increased. In addition, Wnt1 induction resulted in a decreased pulp volume due to ectopic formation of calcified material in the pulp cavity. Thus, Wnt1 has an active influence on tooth and alveolar bone formation in growing mice.

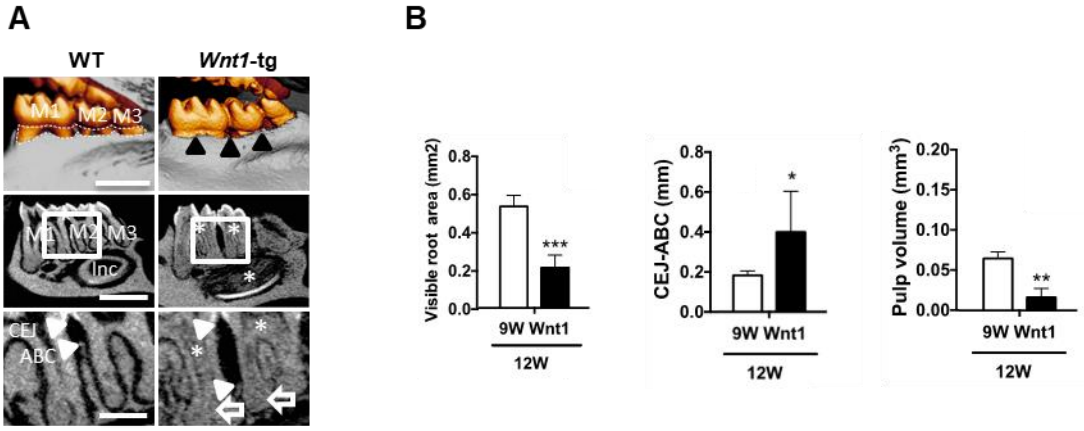

Figure 1.6 Wnt1 induction affects teeth and alveolar bone in growing mice. A) µCT imaging of mandibular molars with cross-sections from 12-week-old male (9 weeks after induction of the transgene) control and Wnt1-transgenic mice of lower incisors (lower panels). The visible root area (dashed white lines) and the distance between the cementum-enamel-junction and the alveolar bone crest (white triangles) were measured as surrogate markers for alveolar bone formation. Note that calcified tissue is present in the pulp chambers of molars and incisors (white asterisks). B) Quantification of the visible root area, the distance between the cementum-enamel-junction and the alveolar bone crest (CEJ-ABC) and the pulp volume. n≥4. Data are the means ± SEM. ***P < 0.001; **P < 0.01; *P < 0.1.

The major aim of this thesis was to define the influences of Wnt1 on bone and teeth in 1-year-old mice (9 weeks after induction of the transgene). This was particularly relevant, since Wnt1 is a potential anabolic drug target for the treatment of osteoporosis, which is much more frequent in elderly individuals as well as for the treatment of osteogenesis imperfecta (OI) a group of rare developmental diseases characterized by improper mineralization of bone leading to bone fragility.

2. Material and Methods

2.1 Material

2.1.1 Equipment

Equipment	Model	Manufacture
Autoclave	5050ELC	Tondauer Europe B.V. (Breda, NL)
Ice Cube Machine	FM-120DE	Hoshizaki Denki K.K. (Toyoake, JP)
Competence Analytical Balance	CPA224S	Sartorius AG (Göttingen, DE)
TE Top-Loading Balances	TE2101	Sartorius AG (Göttingen, DE)
Gel documentation Image System	E-Box VX2	Peqlab Biotechnologies GmbH (Erlangen, DE)
Sub-Cell GT Electrophoresis Cell	Sub-Cell GT	Bio-Rad Laboratories, Inc. (Hercules, US)
Incubator	BBD 6220	Heraeus Holding GmbH (Hanau, DE)
Camera	50 mm 1:2.8 DG Macro	Sigma (Kanagawa, JP)
Lightbox	1634	Hama GmbH & Co KG (Monheim, DE)
Magnetic Stirrer	RCT Basic	IKAR-Werke GmbH & CO. KG (Staufen, DE)
Microtiter plate reader	Versamax	Molecular Devices, LLC (Sunnyvale, US)
Electrophoresis Power Supplies	200/2.0	Bio-Rad Laboratories, Inc. (Hercules, US)
PCR-System	Mastercycler pro S	Eppendorf AG (Hamburg, DE)
PCR-System	Mastercycler epgradient S	Eppendorf AG (Hamburg, DE)

Equipment	Model	Manufacture
pH/ORP Meter	HI 2211 pH/ORP Meter	Hanna Instruments (Woonsocket, US)
Pipetting	Pipetboy acu	INTEGRA Biosciences AG (Zizers, CH)
Real-Time PCR System	StepOnePlus	Applied Biosystems, Inc. (Foster City, US)
Safety Cabinet	HS12	Heraeus Holding GmbH (Hanau, DE)
Safety Cabinet	Msc-Advantage	Thermo Fisher Scientific, Inc. (Waltham, US)
Spectrophotometer	Nanodrop ND1000	Peqlab Biotechnologies GmbH (Erlangen, DE)
Dry Block Incubator	Thermostat Plus	Eppendorf AG (Hamburg, DE)
Thermomixer	Comfort	Eppendorf AG (Hamburg, DE)
Thermomixer	5436	Eppendorf AG (Hamburg, DE)
Tabletop Centrifuge	5425	Eppendorf AG (Hamburg, DE)
Tabletop Centrifuge	5430R	Eppendorf AG (Hamburg, DE)
Tabletop Centrifuge	5415D	Eppendorf AG (Hamburg, DE)
Vortex mixer	Reax top	Heidolph Instruments, GmbH & Co. KG (Schwabach, DE)
Water Bath	1012	GFL Gesellschaft für Labortechnik mbH (Burgwedel, DE)
Centrifuge	GS-6	Beckman Coulter, Inc. (Brea, US)

Equipment	Model	Manufacture
X-ray microcomputer tomograph	µCT 40	Scanco Medical AG (Brüttisellen, CH)
Western Blotting Equipment	Trans-Blot® Plus	Bio-Rad Laboratories, Inc. (Hercules, US)
X-ray Film Processor	Protec Optimax	Raytech Diagnostics (Ottawa , CAN)
VersaMax Microplate Reader	S/N B 02410	Molecular Devices (Sunnyvale, US)
Embedding	TES 99	MEDITE (Burgdorf, DE)
Microtome Leica RM2245 - semi-automatic microtome	CA RM2245	Leica Biosystems Nussloch GmbH (Nussloch, DE)
Waterbath	Pfm Waterbath 1000	Pfm medical Quality and Experience (Köln, DE)
Microscope	IX50	Olympus (Tokio, JP)
Vacuum Pump	PC 2004 VARIO	VACUUBRAND GMBH + CO KG(Wertheim, DE)
Platform shaker	1030	Heidolph Instruments GmbH & CO. KG (Schwabach, DE)

2.1.2 Consumables

Consumables - Designation	Manufacturer
BD Eclipse™ Needle with SmartSlip™ Technology (0.8mmx40mm)	BD GmbH (Heidelberg, DE)
Biosphere® Filter Tips 100-1000 µL	Sarstedt AG & Co. (Nümbrecht, DE)
Biosphere® Filter Tips 2-100 µL	Sarstedt AG & Co. (Nümbrecht, DE)
Biosphere® Filter Tips 0,1-10 µL	Sarstedt AG & Co. (Nümbrecht, DE)
Cell Culture Dishes, PS, 100x20 mm, with vents, sterile	Greiner Bio-One International AG (Kremsmünster, AT)

Consumables - Designation	Manufacturer
Cell Culture Flasks, 250 ml, 75 cm^2, PS, red standard cap, sterile	Greiner Bio-One International AG (Kremsmünster, AT)
Cell Scraper, 25 cm	Sarstedt AG & Co. (Nümbrecht, DE)
Disposable Glass Pasteurpipettes 230 mm	VWR International, LLC (Radnor, US)
Gewebekulturschalen 60/15 mm, steril	Greiner Bio-One International AG (Kremsmünster, AT)
Injekt® 10 ml steril	B. Braun Melsungen AG (Melsungen, DE)
Labsolute® single use filter unit 0.20 µm	Th. Geyer GmbH & Co. KG (Hamburg, DE)
MicroAmp® Fast 96-Well Reaction Plate (0.1 ml)	Thermo Fisher Scientific, Inc. (Waltham, US)
MicroAmp™ Optical Adhesive Film	Thermo Fisher Scientific, Inc. (Waltham, US)
PCR SingleCap 8er-SoftStrips 0.2 ml	Biozym Scientific GmbH (Hessisch Oldendorf, DE)
PCR 12er-SoftStrips, 0.2 ml, mixed colors	Biozym Scientific GmbH (Hessisch Oldendorf, DE)
Quality Pipette Tips 100-1000 µL	Sarstedt AG & Co. (Nümbrecht, DE)
Quality Pipette Tips 2-200 µL	Sarstedt AG & Co. (Nümbrecht, DE)
Quality Pipette Tips 0.1-10 µL	Sarstedt AG & Co. (Nümbrecht, DE)
Reagent tube 1.5 ml SafeSeal	Sarstedt AG & Co. (Nümbrecht, DE)
Reagent tube 2.0 ml SafeSeal	Sarstedt AG & Co. (Nümbrecht, DE)
Serological pipette 5 ml, sterile	Sarstedt AG & Co. (Nümbrecht, DE)
Serological pipette 10 ml, sterile	Sarstedt AG & Co. (Nümbrecht, DE)
Serological pipette 25 ml, sterile	Sarstedt AG & Co. (Nümbrecht, DE)
Tissue Culture Plate, 12 Well, Flat Bottom with Low Evaporation Lid, sterile	Corning, Inc. (New York, US)

Consumables - Designation	Manufacturer
Tubes, 15 ml, PP, graduated, conical bottom, blue screw cap, sterile	Greiner Bio-One International AG (Kremsmünster, AT)
Tubes, 50 ml, PP, graduated, conical bottom, blue screw cap, sterile	Greiner Bio-One International AG (Kremsmünster, AT)
Sterile Scalpel Blade	C. Bruno Bayha (Tuttlingen, DE)
6 Well Cell Culture Plate sterile, with lid	Greiner Bio-One International AG (Kremsmünster, AT)
12 Well Cell Culture Plate sterile, with lid	Greiner Bio-One International AG (Kremsmünster, AT)
Cryo.s™, PP, with scrow cap, sterile	Greiner Bio-One International AG (Kremsmünster, AT)
Hybond LFP-PVDF Westernblot-Membran	GE Healthcare Ltd. (Little Chalfont, UK)
Cover glasses	
Microscope Slides	
Amersham Hyperfilm™ MP High performance autoradiography film	GE Healthcare Limited

2.1.3 Chemicals

Name	Abbreviation	Molecular formula	Manufacturer
Agarose (SeaKem® LE)		$[C_{12}H_{18}O_9]_n$	Lonza Group AG (Basel, CH)
Ammoniumperoxodisulfat	APS	$H_8N_2O_8S_2$	Sigma-Aldrich Corp. (St. Louis, US)
Ammoiumhydroxid		NH_3	Sigma-Aldrich Corp. (St. Louis, US)
Diethylpyrocarbonat	DEPC	$C_6H_{10}O_5$	Sigma-Aldrich Corp. (St. Louis, US)

Name	Abbreviation	Molecular formula	Manufacturer
Dimethyl sulfoxide	DMSO	C_2H_6OS	Carl Roth GmbH & Co. KG (Karlsruhe, DE)
Acetic Acid		$C_2H_4O_2$	Carl Roth GmbH & Co. KG (Karlsruhe, DE)
Ethidiumbromid	EtBr	1239-45-8	Sigma-Aldrich Corp. (St. Louis, US)
Ethylendiamintetraacetat	EDTA	$C_{10}H_{16}N_2O_8$	Merck KGaA (Darmstadt, DE)
G418-BC		$C_{20}H_{40}N_4O_{10} \cdot 2H_2SO_4$	Biochrom GmbH (Berlin, DE)
2-Propanol	Isopropanol	C_3H_8O	Carl Roth GmbH & Co. KG (Karlsruhe, DE)
L-ascorbic acid	ASC	$C_6H_8O_6$	Sigma-Aldrich Corp. (St. Louis, US)
Natriumchlorid	NaCl	NaCl	Sigma-Aldrich Corp. (St. Louis, US)
Natrium-3,3-dihydroxy-9,10-dioxo-2-anthracenesulfonat	Alizarinrot S	$C_{14}H_7NaO_7S$	Chroma GmbH Co. KG (Münster, DE)
Tris(hydroxymethyl)aminomethanhydrochlorid	Tris/HCl	$NH_2C(CH_2OH)_3 \cdot HCl$	Sigma-Aldrich Corp. (St. Louis, US)
Tris(hydroxymethyl)aminomethan	Tris Base	$NH_2C(CH_2OH)_3$	Carl Roth GmbH & Co. KG (Karlsruhe, DE)
β-Glycerophosphat	β-Gly	$C_3H_7Na_2O_6P$	Sigma-Aldrich Corp. (St. Louis, US)
β-Mercaptoethanol		C_2H_6OS	Sigma-Aldrich Corp. (St. Louis, US)
Wasserstoffperoxid		H_2O_2	Merck KGaA (Darmstadt, DE)
Glycin	Gly	NH_2CH_2COOH	Carl Roth GmbH + Co. KG (Karlsruhe, DE)

Name	Abbreviation	Molecular formula	Manufacturer
Tetramethylethylendiamin	TEMED	$C_6H_{16}N_2$	Sigma-Aldrich Corp. (St. Louis, USA)
Sodium lauryl sulfate	SDS	$C_{12}H_{25}NaO_4S$	Carl Roth GmbH & Co. KG (Karlsruhe, DE)
Ethanol	EtOH	C_2H_6O	Merck KGaA (Darmstadt, DE)
Dithiothreitol	DTT	$C_4H_{10}O_2S_2$	Sigma-Aldrich Corp. (St. Louis, USA)
Propan-1,2,3-triol	Glycerin	$C_3H_8O_3$	Carl Roth GmbH & Co. KG (Karlsruhe, DE)
Methanol	MeOH	CH_4O	Carl Roth GmbH & Co. KG (Karlsruhe, DE)
Tween®20		$C_{58}H_{114}O_{26}$	Carl Roth GmbH & Co. KG (Karlsruhe, DE)
Chloroform		$CHCl_3$	Sigma-Aldrich Corp. (St. Louis, USA)

2.1.4 Finished solutions and Powders

Finished solutions and Powders	Description	Manufacturer
DNA-Größenstandard	GeneRuler 1kb Plus DNA Ladder	Thermo Fisher Scientific, Inc. (Waltham, US)
dNTP-Mischung	dNTP-Mix, 10mM	Thermo Fisher Scientific, Inc. (Waltham, US)
Ethanol	Ethanol 80 % vergällt mit MEK, Bitrex®, IPA	Th. Geyer GmbH & Co. KG (Hamburg, DE)
Fetal Bovine Serum (Hyclone, RYL35914)	Fetal calf serum for osteoblasts (FKS Obl)	Thermo Fisher Scientific, Inc. (Waltham, US)
Lipofectamin LTX und Plus™ Reagent	Plasmid Transfection Reagent	Thermo Fisher Scientific, Inc. (Waltham, US)

Finished solutions and Powders	Description	Manufacturer
PhosSTOP	Phosphatase-Inhibitoren	Roche Diagnostics GmbH. (Mannheim, DE)
Complete Tablets EDTA-free, EASYpack	Protein isolation	Roche Diagnostics GmbH. (Mannheim, DE)
Penicillin-Streptomycin (10,000 U/mL)	Penicillin-streptomycin mixture	Thermo Fisher Scientific, Inc. (Waltham, US)
DMEM-Medium	DMEM (1x) + GlutaMAX^{TM} -1	Thermo Fisher Scientific, Inc. (Waltham, US)
Fetal Bovine Serum	Fetal calf serum (Obl)	Thermo Fisher Scientific, Inc. (Waltham, US)
SYBR Green Mix	Fast SYBR^{TM} Green Master Mix	Thermo Fisher Scientific, Inc. (Waltham, US)
TaqMan Mix	TaqMan^{TM} Gene Expression Master Mix	Thermo Fisher Scientific, Inc. (Waltham, US)
Trypsin-EDTA	0.25 % Trypsin-EDTA (1x)	Thermo Fisher Scientific, Inc. (Waltham, US)
Steriles Wasser	Water, DEPC-treated and sterile filtered	Sigma-Aldrich Corp. (St. Louis, US)
α-MEM Cell culture medium	Minimum Essential Medium Eagle Alpha Modification	Sigma-Aldrich Corp. (St. Louis, US)
PBS (1x)	Gibco® DPBS (1x) Dulbecco's Phosphate-Buffered Saline	Thermo Fisher Scientific, Inc. (Waltham, US)
Rotiphorese® Gel 30 (37,5:1)	aqueous 30% acrylamide, bisacrylamide stock solution in the ratio 37.5: 1	Carl Roth GmbH & Co. KG (Karlsruhe, DE)
PeqGOLD TriFast	RNA isolation solution	VWR International GmbH(Darmstadt, DE)
Albumin Standard 2 mg/mL	BSA stock solution	Thermo Fisher Scientific Inc. (Waltham, US)

Finished solutions and Powders	Description	Manufacturer
Phenol:Chloroform:Isoamyl Alcohol	DNA Isolation solution	Carl Roth GmbH & Co. KG (Karlsruhe, DE)

2.1.5 Protein

Name	Manufacturer
Bovine Serum Albumin (BSA)	Sigma-Aldrich Corp. (St. Louis, USA)

2.1.6 Kits and assays

Usage	Kit/Assay	Manufacturer
cDNA Synthese	Verso cDNA Synthesis Kit	Thermo Fisher Scientific, Inc. (Waltham, US)
Wnt1-ELISA	Mouse Proto-oncogene Wnt-1(WNT1) ELISA kit	Cusabio Wuhan Huamei Biotech Co., LTD. (Wuhan, CN)
Western Blot detection	Pierce^{TM} ECL Western Blotting Substrate	Thermo Fisher Scientific, Inc. (Waltham, US)

2.1.7 Buffers and solutions

In all experiments of this work deionized H_2O was used.

Solution/Buffer	Composition	
Alizarin Red staining solution	40 mM	Alizarinrot S ad. H_2O pH 4.2

Solution/Buffer	Composition	
Ampicillin stock solution	100 mg/mL	Ampicillin ad. H_2O steril filtriert
Block buffer		5% BSA in 1x TBST
DEPC-H_2O	0.2 % (v/v)	Proteinase-K ad. H_2O
Tail lysis buffer	2.5 mM 50 mM 100 mM 0.1 % (w/v)	EDTA Tris/HCl NaCl SDS ad. H_2O pH 8.5
TAE buffer (50x)	2.5 mM 50 mM	Tris/HCl EDTA ad. H_2O pH 7.8
TE buffer	10 mM 1 mM	Tris/HCl EDTA ad. H_2O pH 7.5
Separating gel buffer	1.5M 0.4%	Tris/HCl SDS ad. H_2O pH 8.8

Solution/Buffer	Composition	
Tris	70 mM	Tris Base
		ad. H_2O
Collection gel buffer	1.5M	Tris/HCl
	0.4%	SDS
		ad. H_2O
		pH 6.8
Coomassie staining solution	0.1%	Coomassie T250
	40%	Methanol
	1%	Acetic acid
4x Sample buffer	500mM	Tris/HCl
	0.4%	SDS
	40%	Glycerin
	40mM	DTT
		ad. H_2O
		pH 6.8
10x Running buffer	10x 25mM	Tris-Base
	10x 25mM	Glycerin
	10x 0.1%	SDS
		ad. H_2O
10x TBS buffer	500mM	Tris/HCL
	1500mM	NaCl
		ad. H_2O
		pH 7.4

Solution/Buffer	Composition	
β-glycerophosphate stock solution	2 M	β-Glycerophosphat
		ad. H_2O
TBST buffer		TBS buffer
	0.1%	Tween20
		ad. H_2O
NET-buffer	50mM	Tris/HCL
	150mM	NaCl
	5mM	ETDA
	0.05%	TRITON-X-100
	0.25%	Gelatine
		ad. H_2O
ECL chemiluminescence solution	0.1M	Tris
	30%	H_2O_2
	500mM	Luminol
	80mM	p-coumaric acid
RIPA buffer	1 % (v/v)	NP-40
	1 % (v/v)	Natriumdesoxycholat
	0.1 % (w/v)	SDS
	150 mM	NaCl
	2 mM	EDTA
	10 mM	Natriumphosphat
		ad. H_2O
		pH 7.4

2.1.8 Antibodies for Western Blots

Target	Source	Manufacturer	Product Number	Dilution
β-Actin	Rabbit	Cell Signaling	#4967	1:1000
HA-Tag	Mouse	Cell Signaling	#2367	1:1000
β-Catenin	Rabbit	Cell Signaling	#8480	1:1000
Non-phospho β-Catenin	Rabbit	Cell Signaling	#19807	1:1000
Phospho-S6 Ribosomal Protein	Rabbit	Cell Signaling	#2211	1:1000
Cyclin D1	Mouse	Cell Signaling	#2926	1:2000

2.1.9 TaqMan probes

Gene	TaqMan®Probes
Apcdd1	Mm01257559_m1
Alpl	Mm00475834_m1
Ank	Mm00445050_m1
Axin2	Mm00443610_m1
Bglap1	Mm03413826_mH
Ccnd1	Mm00432359_m1
Ctnnb1	Mm00483039_m1
Myc	Mm00487804_m1
Enpp1	Mm00507097_m1
Fosl1	Mm04207958_m1
Gapdh	4352661

Gene	TaqMan®Probes
Lrp5	Mm01227476_m1
Lrp6	Mm00999795_m1
Phex	Mm00448119_m1
Ibsp	Mm00492555_m1
Spp1	Mm00450403_g1
Wnt1	Mm01300555_g1

2.1.10 SYBR Green Primer

Name	Sequence (5’ – 3’)
Gapdh_for	GACATCAAGAAGGTGGTGAAGCAG
Gapdh_rev	CTCCTGTTATTATGGGGGTCTGG
Wnt1-HA_neu_fw	CCACTGCACCTTCCACTGG
HA_rev	TCTGGGACGTATGGGTA
Myc_neu_fw	CGCGATCAGCTCTCCTGAAA
Myc_neu_rev	GCTGTACGGAGTCGTAGTCG

2.1.11 Used Programs

Programm	Version	Manufacturer
Microsoft Office 2010	14.0	Microsoft Corp. (Redmond, US)
Serial Cloner	2-6-1	Serial Basics
EndNote	X7.3.1	Clarivate Analytics (Jersey)
Fiji(ImageJ)	1.48p	Schindelin et al., 2012[251]
BoneJ	01.03.2011	Doube et al., 2010[252]

Programm	Version	Manufacturer
MicroCT Software Suite	4.05	Scanco Medical AG (Brüttisellen, CH)
GraphPad Prism	6	Graph Pad Software, Inc. (La Jolla, US)
StepOne™ Software	2.3	Applied Biosystems, Inc. (Foster City, US)
ND-1000	3.5.2	Thermo Fisher Scientific, Inc. (Waltham, US)
SOFTmax PRO	3.1.2	Molecular Devices, LLC (San José, US)

2.2 Methods

2.2.1 Micro-computed tomography

Micro-computed tomography (micro-CT or µCT) uses X-ray to create two-dimensional (2D) trans-axial projections, to compose high-resolution three-dimensional (3D) images in a non-destructive way. With the help of this method, the trabecular bone, cortical bone and teeth can be restructured and analyzed for relevant parameters.

The right femur was dissected from the fixed mice and fixed in the holder (Φ20mm*H75mm). The holder was placed in a µCT 40 (Scanco Medical AG) with a voxel resolution of 10 µm. Anatomical separation of the skull was performed in the same way, but a different holder was used (Φ30mm*H75mm).

3D models were made with the manufacturer's scripts "UCT_EVALUATION", and pictures were generated by the program µCT Ray V3.8 from the same software suite.

Analysis of the trabecular bone was performed from the distal metaphysis in a volume situated 2500 µm to 500 µm proximal of the distal growth plate, whereas the cortical bone was analyzed in a 1000 µm long volume situated in the middle of the diaphysis. This allowed the determination of the following parameters:

BV/TV: Trabecular bone volume (bone volume per tissue volume), a parameter for the bone density.

Tb.Th: Trabecular thickness, a parameter for the average diameter of single trabeculae.

Tb.N: Trabecular number, a parameter for the number of trabeculae.

Cort.Th: Cortical thickness, a parameter for thickness of cortical bone.

2.2.2 Histology

2.2.2.1 Acrylate histology

The acrylate histology is well suited for bone tissue samples for histological analysis. This technique can retain important information on bone turnover, bone formation, and bone resorption. Acrylate histology sectioning allows different staining techniques.

The lumbar vertebral bodies L1-L4 were prepared and dehydrated in ascending alcohol (EtOH) concentrations (1-5 h 70% EtOH, 1h 70% EtOH, 2 x 1h 80% EtOH, 4 x 1h 96% EtOH, 4x 100% EtOH). Afterwards, the specimens were sequentially placed in two infiltration solutions at 4°C each for 24 hours each. The specimens were then embedded in methyl methacrylate solution containing 0.5% (v / v) DMPT (as a starter for the polymerization process) in roll rims glass. After the polymerization process completed at 4°C, the sample block was carefully released from the glass. Sections of 4 µm thickness (for structural and cellular histomorphometry) and 12 µm (for dynamic histomorphometry) were cut on a rotary microtome (Cambridge Instruments Co. Ltd.) with special blades for acrylate histology. The sections were stretched by brushes with 80% isopropyl alcohol and dibutyl ether, then covered with a piece of polyethylene foil and tightened the press and let dry over-night at 60°C.

2.2.2.2 Paraffin Histology

First, decalcified skull specimens were prepared. The skulls were placed into the 10% EDTA (pH7.4) for at least 4 weeks, the solution being changed every week. After the decalcification samples were ready, they were cut into no more than 3mm thick slices and dehydrated in ascending alcohol concentrations before embedding. The process for embedding tissues into paraffin blocks was as follows: 1h 70% EtOH, 1h 80% EtOH, 2 x 1h 96% EtOH, 2 x 1h 100% EtOH, 2 x 1h Xylene, 2 x 2h Paraffin wax (58-60°C). After the samples in paraffin were dried, sections of 3.5 µm were cut on a semi-automated rotary microtome (Leica Biosystems Nussloch GmbH). Sections were allowed to air dry for 30 minutes and then baked in 38 °C oven overnight.

2.2.2.3 Histologic staining

2.2.2.3.1 Von Kossa/ van Gieson staining

Combined von Kossa and van Gieson staining allow clear identification of undecalcified bone. The von Kossa staining leads to black coloring of calcium-deposits, while after van Gieson staining collagen tissues are purple-red; smooth and striated muscle and erythrocytes are yellow. For staining of 4 µm thick sections the following protocol was

used: 3 x 5 min deplaster (2-methoxyethyl acetate), 2 x 100 min EtOH, 2 min 96% EtOH, 2 min 80% EtOH, 2 min 70% EtOH, 2 min 50% EtOH, 3-5 x wash with H_2O, 5 min Kossa color solution, 10 min running tap water, 5 minutes of soda foam solution, 10 minutes running tap water, 5 min Sodium thiosulfate solution, running tap water for 10 min, Gieson color solution for 20 min, short running tap water, short 80% EtOH, short 96% EtOH, 2x short 100% EtOH, 3x 5 min Xylene. Subsequently, coverslips were covered with DPX mounting medium.

2.2.2.3.2 Toluidine Blue staining

Toluidine blue staining is a well-established method for the histological evaluation of cartilage and chondrogenic-differentiated tissues. The coloring of 4 µm thick sections was done following the protocol: 3 x 5 min Deplaster, 2 x 2 min 100% EtOH, 2 min 96% EtOH, 2 min 80% EtOH, 2 min 70% EtOH, 2 min 50% EtOH, wash 3-5 x with H_2O, toluidine color solution for 30 min, wash with H2O, wash with 50% EtOH, 2 min 70% EtOH, 2 min 80% EtOH, 2 min 96% EtOH, 5 min 100% EtOH, wash with 100% EtOH, 3 x 5 min Xylene. Finally, coverslips were covered with DPX mounting medium.

2.2.2.3.3 Hematoxylin and eosin stain (H&E stain)

H&E is a combination of histological staining, where hematoxylin stains cell nuclei blue, and eosin stains the extracellular matrix and cytoplasm pink. The protocol for staining of 3.5 µm sections consisted of the following steps: 3 x 5 min Xylol, 2 x 2 min Ethanol abs., 2 min 96% EtOH, 2 min 80% EtOH, 3-5 x dip wash in distilled water. , 5 min Mayer's hemalum solution, rinse briefly by distilled water, 2-3 x dip wash in 0.1% HCL–alcohol, 10 min blue (fluent water or change water), 5 min 0.1% Eosin, rinse briefly by 80% EtOH, 2 min 96% EtOH, 2 x 2 min Ethanol abs., 3 x 5 min Xylol, coverslips were covered with DPX mounting medium.

2.2.2.4 Histomorphometry

Bone histomorphometry is a technique for quantitative analysis of bone architecture, which provides a two-dimensional representation of a three-dimensional structure.

2.2.2.4.1 Static Histomorphometry

Static histomorphometry allows assessing structural and cellular variables on histologic sections at a particular time point. For the trabecular area in the vertebrae L4 and L3 in von Kossa/ van Gieson-colored sections the structural parameters were quantified semi-automatically with the Bioquant Osteo software. This allowed the determination of the following measured values:

BV/TV: Trabecular bone volume (bone volume per tissue volume), a parameter for the bone density.

Tb.Th: Trabecular thickness, a parameter for the average diameter of single trabeculae.

Tb.N: Trabecular number, a parameter for the number of trabeculae.

The cellular characteristics of the bone were measured the trabecular area of the vertebral body L4 in toluidine blue-stained sections using the Osteomeasure software.

The specific perimeter has defined to analyze the histological sections were:

N.Ob/B.Pm: Number of osteoblasts per bone perimeter, a parameter for the osteoblast cell number relative to the actual amount of bone.

N.Oc/B.Pm: Number of osteoclasts per bone perimeter, a parameter for the osteoclast cell number relative to the actual amount of bone.

Ob.S/BS: Osteoblast surface per bone surface, a parameter for the bone surface that is occupied by osteoblasts.

Oc.S/BS: Osteoclast Surface per bone surface, a parameter for the bone surface that is occupied by osteoclasts.

2.2.2.4.2 Dynamic Histomorphometry

Dynamic histomorphometry, the standard method for understanding bone remodeling, allows measurement of bone formation rates. The calcein-labeled specimens were measured in the trabecular area of the L4 vertebral body with the Osteomeasure software. The fluorescent calcein dye (Excitation 495 nm, emission 515 nm) was visible with appropriate filter systems. The following measured value was determined:

BFR/BS: Bone formation rate per unit of bone surface, a parameter for osteoblast activity.

2.2.3 ImageJ and BoneJ

ImageJ is an open source Java image processing program with thousands of plugins and macros for performing a wide variety of tasks. BoneJ is a plugin for bone image analysis in ImageJ. This allowed the determination of the following parameters:

Visible root area: Mandibular molars (M1, M2, and M3) buccal side root visible area.

Distance: The length between the cementum-enamel-junction and the alveolar crest.

Calvarial thickness: The means of the skull thickness in the skull coronal section.

Calvarial porosity: The void spaces in the calvarial bone of the skull coronal section. It's a fraction of the volume of voids over the total volume, as a percentage between 0% and 100%.

2.2.4 Cell culture

2.2.4.1 OCCM cells culture

Culture of OCCM cells: The cementum cell line OCCM was cultured in Dulbecco's Modified Eagle Medium (DMEM + GlutaMAX^{TM}-1) containing 10% Fetal Bovine Serum (FBS), and 1% Penicillin/Streptomycin at 37 °C in an atmosphere containing 5% CO_2. The medium was changed every two days.

2.2.4.2 Stable transfection and selection

Transfection is the process of introducing a foreign nucleic acid into eukaryotic cells. OCCM cells were transfected with the pLNCX control vector and the Wnt1a plasmid with Lipofectamine LTX and Plus reagent. First, 1 x 105 OCCM cells were seeded in a 6-well plate and grown until 70-90% confluency. Subsequently, I prepared diluted Lipofectamine® LTX mixture and diluted DNA (with PLUS™) mixture as indicated in Table 1. Diluted DNA and diluted Lipofectamine® LTX reagent were mixed in a 1:1 ratio and incubated for 5 minutes at room temperature. 250 µl of DNA-lipid complex were added to OCCM cells and cells were incubated for 1 day at 37 °C.

Table 1. Transfection reagent (1x) for 6-well plate

Component	Volume (µl) 1x
DMEM without Serum Medium	125 µl
Lipofectamine® LTX Reagent	7.5 µl
DMEM without Serum Medium	125 µl
DNA	2.5 µg
PLUS™ Reagent	2.5 µl
Diluted DNA (with PLUS™ Reagent) Total	125 µl
Diluted Lipofectamine® LTX Reagent	125 µl

After 24h, cells were split from 6-well plate into 10cm dishes and were put directly into the selective media (DMEM +/+, G418-BC: 10µl/ml). Geneticin™ Selective Antibiotic (G418-BC) blocks polypeptide synthesis and protein elongation by inhibiting synthesis at the 70S and 80S ribosomes. One dish of untransfected cells was treated by the same way (splitting into selective media) to ensure that the antibiotic is working effectively and that the untransfected cells died during the selection. Normally, the selection step requires 2-3 cell passages and the OCCM transfected cells were used in subsequent experiments.

2.2.5 Molecular biology methods

2.2.5.1 Cell number determination

The OCCM cells were diluted to a suitable concentration. 10µl OCCM cell suspension was pipetted in a Neubauer chamber. In order to accurately count the number, two out of 4 corner squares were employed to take the average cell count from each of the sets. The counted number was multiplied by 10,000 (10^4) and the dilution ratio. The unit is per milliliter.

2.2.5.2 RNA isolation from cultured cells

To purify the OCCM cell RNA, the next steps were followed: The cells were first mixed with the lysis reagent peqGOLD TriFast™ and incubated 5 minutes at room temperature, then detached from the cell culture plates with cell scrapers. The mixture was pipetted into the micro-tube which contained phenol/chloroform (0.3ml of phenol/chloroform per 1ml peqGOLD TriFast™ reagent). After being vigorously vortexed, the micro-tube was placed into the centrifuge for 15 minutes at 12,000 x g and 4°C. Subsequently, the supernatant was carefully pipetted to a new micro-tube and thoroughly mixed with 600µl Isopropanol. After been 15 minutes of centrifugation at 12,000 x g and 4°C, the RNA precipitated at the bottom of micro-tube. The pellet was washed with 70% ethanol, dissolved in 50µl H_2O and stored at -80°C.

2.2.5.3 cDNA synthesis

For the synthesis of complementary DNA (cDNA), the Verso cDNA Synthesis Kit (Thermo Fisher Scientific) was used with the following reaction mix:

Table 2. Reaction (1x) of the cDNA synthesis

Reagent	Volume (µl) 1x
5x cDNA Synthesis Buffer	2
dNTP Mix	1
Oligo dT	0,5
Verso Enzyme Mix	0,5
RT Enhancer	0,5
H_2O	3,5
RNA	2

The cDNA was stored at –20°C.

2.2.5.4 Quantitative Real Time PCR

The quantitative Real-Time PCR (qRT-PCR) is the gold standard for detecting target RNA expression with sensitivity and specificity. As part of our experiment, the TaqMan® system and the SYBR® Green system were used. The SYBR® Green system uses to detect the quantities of specific primer sets to amplify the cDNA and SYBR Green I dye for quantification. However with this method also quantifies unspecific reaction products. The TaqMan® system uses in addition to specific primer sets a fluorogenic probe to detect specific amplification products only. The PCR reaction was performed by StepOnePlus™ Real-Time PCR System automatically and calculated by the ΔCT method with glycerinaldehyde-3-phosphate-dehydrogenase (Gapdh) as housekeeping gene. The components of a simple reaction mixture for the quantitative real-time PCR are listed in Table 3.

Table 3. Reaction (1x) of the qRT-PCR (TaqMan and SYBR Green)

Reagent	TaqMan Volume (µl) 1x	SYBR Green Volume (µl) 1x
H_2O	7	7
TaqMan/ SYBR Green Mix	10	10
TaqMan Primer	1	-
Primer1 (2 µM)	-	1
Primer2 (2 µM)	-	1
cDNA (1:5 dilution)	2	1

2.2.5.5 Mineralization analysis

To analyze the influence of Wnt1 in OCCM cells on formation of mineralized matrix, alizarin red staining was performed. After 2 to 12 days of differentiation, cells were washed with 1x PBS, fixed with cold 90% ethanol for 10-15 minutes, washed twice with water, incubated with 40mM alizarin red staining solution at room temperature for 10 minutes, and washed 3-5 times with water. After the cells were photographed on the lightbox, quantification was performed. For this, the stained cultures were incubated for 30 minutes in 800µl 10% acetic acid at room temperature, scraped off and pipetted into a 1.5ml reaction tube, incubated for 5 minutes at 85°C and 2 minutes at 4°C, and then centrifuged for 10 minutes at 13000xg. From the supernatant, 400µl were carefully transferred to a new reaction tube and mixed with 50µl 10% ammonium hydroxide solution. The samples should be adjusted to the pH of 4.1-4. The absorbance was measured at 450nm.

2.2.5.6 Protein isolation

The transfected OCCM cells were lysed with 400 µl radio-immunoprecipitation assay buffer (RIPA buffer) per cell culture dish (⌀10), including protease and phosphatase inhibitors on day 5 of differentiation, scraped off and transferred to 1.5ml reaction tube, incubated at 4°C for 15 minutes, and then centrifuged for 15 minutes at 13000xg and 4°C. The supernatant was pipetted into a new reaction tube, frozen in liquid nitrogen and stored at - 80°C.

2.2.5.7 Protein determination

To determine the concentration of protein, the Bradford test was used, which involves the binding of Coomassie Brilliant Blue G-250 to proteins. First, the standard curve was prepared as indicated in Table 4. The samples were diluted to a total volume of 800µl with H_2O. 200 µl Bradford reagent was then added to each sample or standard and measured at microplate reader at an absorbance of 595nm after 5 minutes incubation. The protein concentration was calculated from a linear standard curve.

Table 4. Component of standard

µl BSA	µl BSA-Solution* 0.2 (mg/ml)	µl H_2O
0	0	800
5	25	775
10	50	750
15	75	725
20	100	700

*60 µl BSA-Solution (2 mg/ml 0.1 M NaOH) + 540 µl H_2O = 0.2 mg/ml

2.2.5.8 SDS -Polyacrylamide gel electrophoresis

Sodium dodecyl sulfate–polyacrylamide gel electrophoresis (SDS-PAGE) is used as a method to separate proteins according to their molecular mass. The 10% SDS-PAGE gel composition is listed in Table 5. 10 µl of protein was mixed with sample buffer, heated for 5 minutes at 95°C and loaded into the wells for separation by electrophoresis at 100-150V.

Table 5. Component of SDS-PAGE Gel

Component	Separation Gel	Stacking Gel
Concentration	10%	
H_2O	6.15ml	4.5ml
Seperation/ Stacking Buffer	3.95 ml	1.875 ml
30 % Acrylamide	5.1 ml	1.125 ml
TEMED	12 µl	15 µl
10 % APS	75 µl	75 µl

2.2.5.9 Western blot

In order to check the expression on protein level, western blot was performed. Western blot is a widely used biochemistry technique for detecting single proteins. To make the proteins available for antibody detection, they are transferred from the SDS-PAGE gel (10%) onto a nitrocellulose membrane. The transfer process was performed using electroblotting at 4°C and 15V overnight. To examine the success of the transfer step, the total protein Ponceau S staining was performed. Subsequently, the nitrocellulose membrane was put into blotting buffer (5% BSA + 95% TBST) for 60 minutes at room temperature, transferred into primary antibody solution overnight at 4°C, washed 3 times with TBST (1X) for 5-10 minutes each time, transferred into secondary antibody solution for 60 minutes at room temperature, washed 3 times with TBST (1X) for 5-10 minutes each time, incubated in ECL western blotting solution for 1 minute and examined by

western blot film in x-ray film processor. The exposure time varied between 30 seconds to 5 minutes.

2.2.5.10 Enzyme-linked immunosorbent assay

An enzyme-linked immunosorbent assay (ELISA) is used to detect proteins in a sample. In this thesis, the mouse proto-oncogene WNT1 ELISA kit was used to detect Wnt1 in the conditioned medium supernatant. In this case, 100 or 200 µl of undiluted cell culture medium was used.

2.2.6 Statistical analysis

Data were generated in triplicate. Means ± error mean in each case are shown. Statistical evaluation was performed by unpaired t-test and two-way analysis of variance. The significance limit was set as $p \leqslant 0.05$.

3. Results

3.1 Effect of Wnt1 induction on bone formation in aged mice

3.1.1 Wnt1 increases trabecular and cortical bone mass in aged mice

Our group has previously shown that an osteoblast-specific induction of Wnt1 expression causes a rapid increase of bone formation (Luther et al. (2018)). To analyze if the same happens in aged mice, Wnt1 expression in 52-week-old female mice was induced (by doxycycline withdrawal) for 9 weeks. µCT imaging clearly illustrated increased trabecular bone mass in femora of Wnt1-transgenic (*Wnt1*Tg) mice (Figure 3.1, A). The quantification of bone volume, trabecular thickness and trabecular number confirmed that *Wnt1*Tg mice have more and stronger trabecular bone than control mice (Figure 3.1, B). The cortical bone of the femora was also analyzed by µCT imaging and quantification, revealing that the cortical thickness was significantly increased in *Wnt1*Tg mice compared to control mice (Figure 3.1, C. D). Therefore, similar to young mice Wnt1 over-expression can induce both, trabecular bone and cortical bone formation in aged mice.

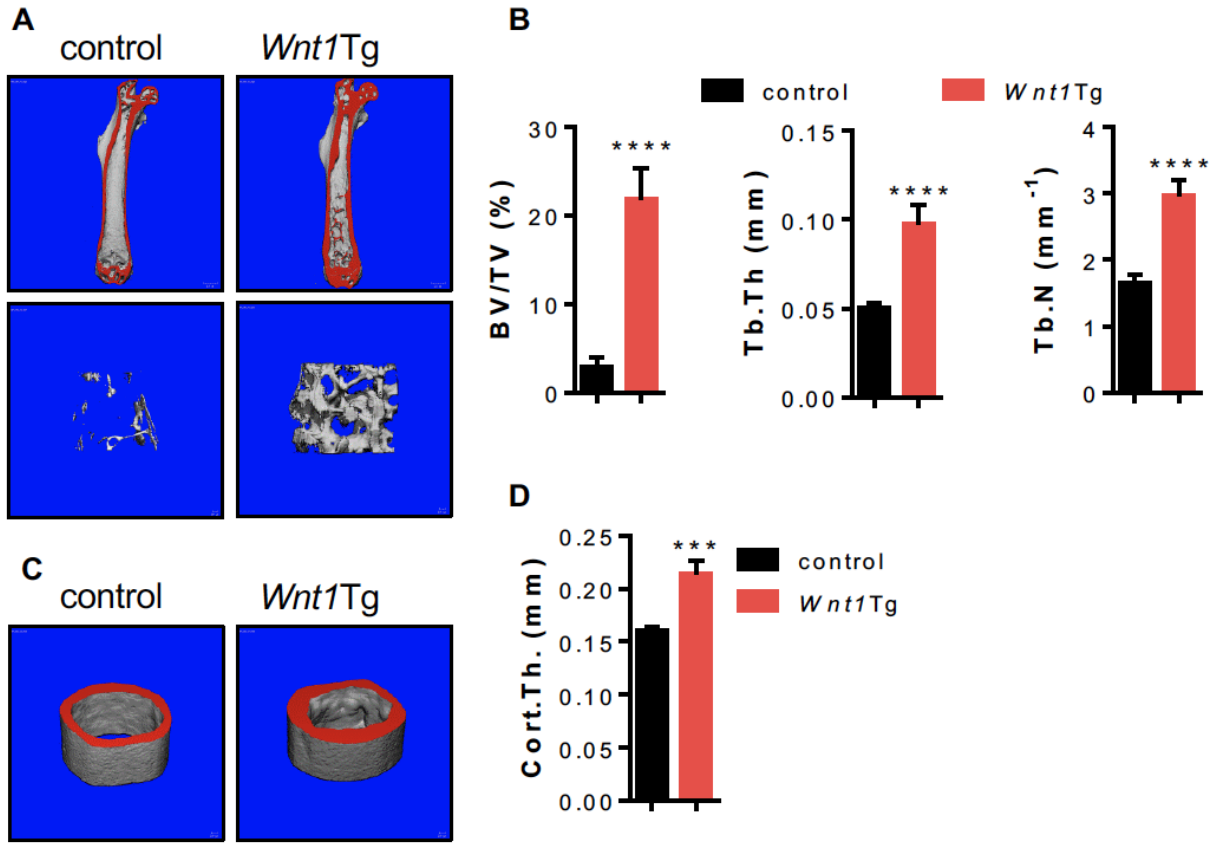

Figure 3.1 Wnt1 increases trabecular and cortical bone mass in aged mice. A) µCT imaging of the femora from 1-year-old control and *Wnt1*-transgenic mice. The trabecular bone was quantified at the distal femoral metaphysis (lower panels). B) µCT quantification of trabecular bone parameters. C) µCT imaging of the femur midshaft from the same mice. D) Quantification of cortical thickness. n≥8. Data are the means ± SEM. ****$P < 0.0001$; ***$P < 0.001$.

3.1.2 Wnt1 induces bone formation in aged mice

Next, we analyzed spine sections by undecalcified histology and bone-specific histomorphometry. The von Kossa/ van Gieson staining of lumbar vertebral bodies L3 and L4 revealed increased bone mass after 9 weeks of Wnt1 induction in 52-week-old female *Wnt1*Tg mice (Figure 3.2, A). This was confirmed by structural histomorphometric results, where bone volume, trabecular thickness and trabecular number were significantly increased in *Wnt1*Tg mice compared to control littermates (Figure 3.2, B). To determine the contribution of osteoblasts and/or osteoclasts, cellular

histomorphometry was performed. The osteoblast surface per bone surface and their number were notably increased in *Wnt1*Tg mice compared to controls (Figure 3.2, C), but there was no difference in the osteoclast surface per bone surface and their number between the two groups (Figure 3.2, D). In addition, dynamic histomorphometric revealed that the bone formation rate was increased in *Wnt1*Tg mice (Figure 3.2, E). These results demonstrated the powerful bone-anabolic function of Wnt1 reported in young mice is also observed in aging mice.

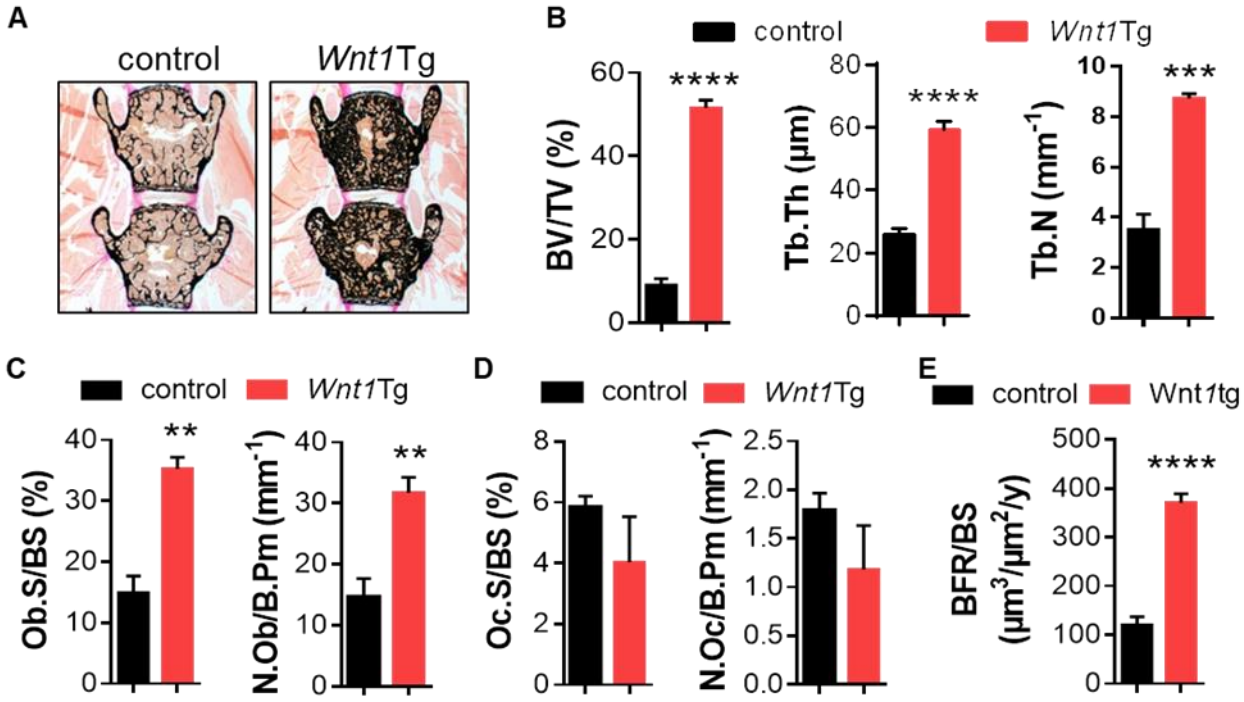

Figure 3.2 Wnt1 induces bone formation in aged mice. A) Von Kossa-stained section of vertebrae from 1-year-old control and *Wnt1*-transgenic (*Wnt1*Tg) mice. Wnt1 was overexpressed in transgenic mice for 9 weeks before sacrifice. B) Histomorphometric quantification of trabecular bone parameters (BV/TV = bone volume per tissue volume, Tb.Th = trabecular thickness and Tb.N = trabecular number). C&D) Histomorphometric quantification of osteoblasts (C) and osteoclasts (D) (Ob.S/BS = osteoblast surface per bone surface, N.Ob/B.Pm = number of osteoblasts per bone perimeter, Oc.S/BS = osteoclast surface per bone surface and N.Oc/B.Pm = number of osteoclasts per bone perimeter). E) Quantification of the bone formation rate per bone surface (BFR/BS). n≥ 3. Data are the means ± SEM. ****$P < 0.0001$; ***$P < 0.001$; **$P < 0.01$.

3.1.3 Wnt1 increases calvarial thickness in aged mice

We were also analysing the potential effect of Wnt1 on intramembranous bone formation. Therefore, we performed µCT scanning of the skull in wild-type and Wnt1Tg mice induced for 9 weeks (Figure 3.3, A). The quantification revealed that the thickness of the calvarial bone was increased in *Wnt1*Tg mice, whereas calvarial porosity was reduced compared to control mice (Figure 3.3, B). These results indicated that Wnt1 also increases intramembranous bone mass in aging mice.

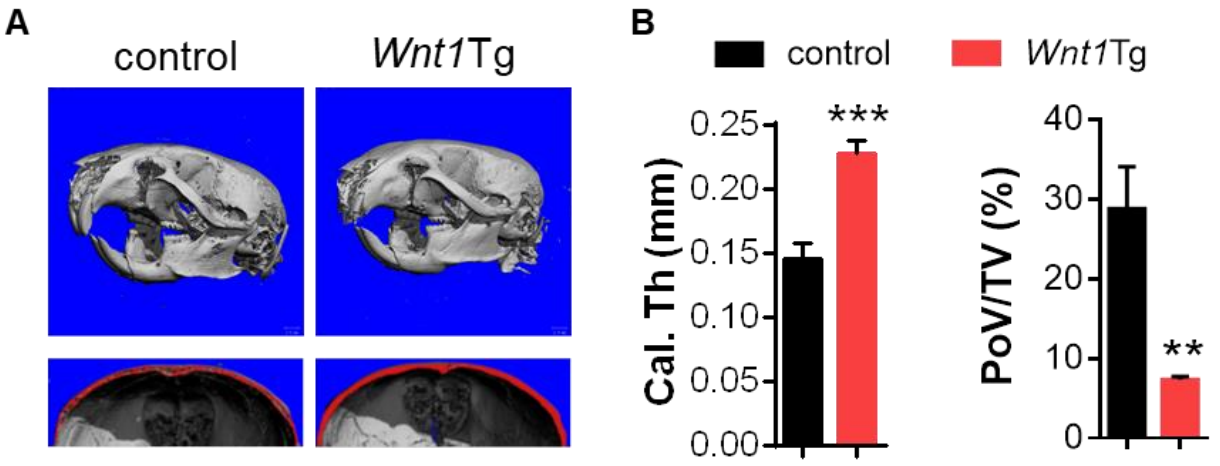

Figure 3.3 Wnt1 induces calvarial bone formation in aged mice. A) µCT imaging of the skull (upper panels) and calvarial bone from 1-year-old control and *Wnt1*-transgenic mice. B) Quantification of the calvarial thickness (Cal.Th) and calvarial porosity (PoV/TV). n≥7. Data are the means ± SEM. ****P* < 0.001; ***P* < 0.01.

3.2 Is Wnt1 induction affecting teeth in aged mice?

3.2.1 Wnt1 does not affect alveolar bone formation in aged mice

We next determined the effect of Wnt1 on the alveolar bone, which is also formed by intramembranous bone formation. We specifically focused on the mandibular alveolar bone in the aging female mice, again using µCT imaging at the region of the mandibular molars (Figure 3.4, A). In that case the quantification did not reveal significant changes. More specifically, the visible root area and distance between the cementum-enamel-junction and alveolar crest was not different between wild-type and *Wnt1*Tg mice (Figure

3.4, B). Importantly however, calcified tissue areas were found inside the pulp chambers of the lower incisors (Figure 3.4, A, lower panels). While these data showed that alveolar bone formation is not increased by Wnt1 induction, the differences in the pulp chambers of growing incisors led us to focus on these teeth in greater detail.

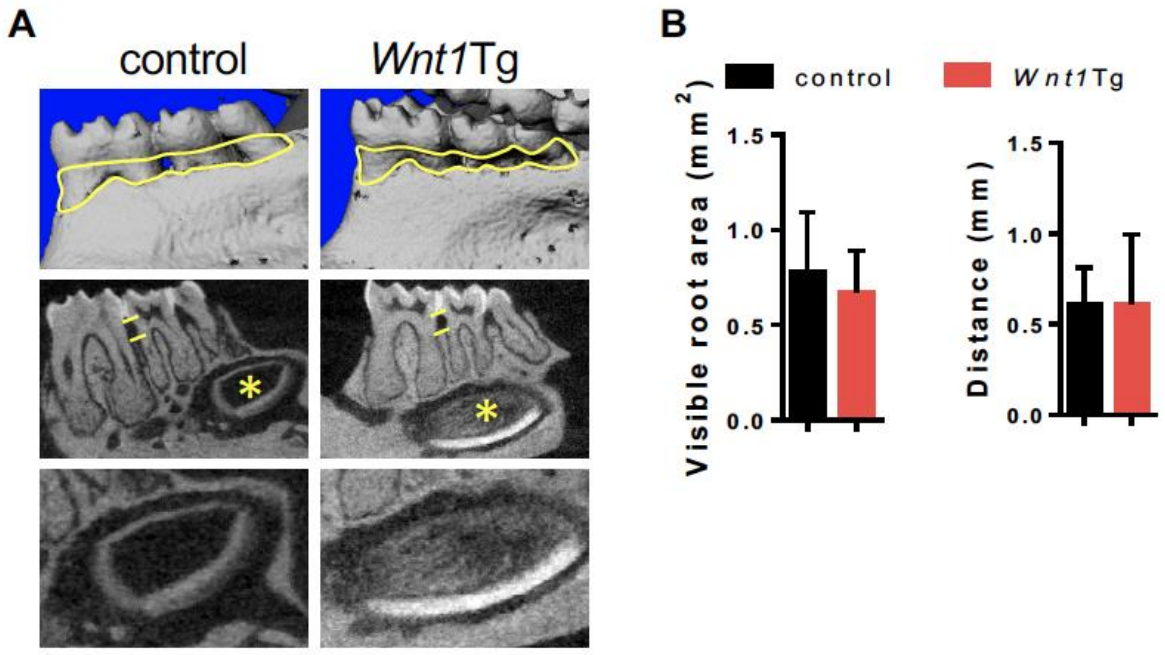

Figure 3.4 Wnt1 does not affect alveolar bone formation in aged mice. A) µCT imaging of mandibular molars with cross-sections of lower incisors (lower panels) from 1-year-old control and *Wnt1*-transgenic mice. The visible root area (yellow circles in upper panels) and the distance between the cementum-enamel-junction and the alveolar crest (yellow lines in middle panels) were measured as surrogate markers for alveolar bone formation. Note that calcified tissue is present only in the pulp chambers of the growing incisors (yellow asterisks). In contrast, molars from *Wnt1*-transgenic mice were unaffected. B) Quantification of the visible root area and the distance between the cementum-enamel-junction and the alveolar crest. n≥5. Data are the means ± SEM.

3.2.2 Wnt1 affects incisor formation in aged mice

Due to the visible change in shape of the maxillary incisors, the upper incisor was scanned by µCT to further clarify the phenotype caused by Wnt1 over-expression in aging mice. µCT 3D-reconstructions of the skull clearly showed shortened upper incisors in *Wnt1*-transgenic mice compared to control mice, and the sagittal cross-sections of

upper incisors confirmed the short incisor phenotype in *Wnt1*-transgenic mice (Figure 3.5, A). µCT quantification showed significant differences between *Wnt1*-transgenic mice and control mice, verifying that the maxillary incisors are shorter in *Wnt1*-transgenic mice than in controls (Figure 3.5, C). To further understand the structural changes in the maxillary incisors, cross-sections at two different positions were examined. In control mice the thickness of the dentin layer decreased from the tip towards the apex. In contrast, *Wnt1*Tg mice exhibited severely disturbed dentin formation (Figure 3.5, B). These results indicated that Wnt1 severely affects incisor growth in aging mice.

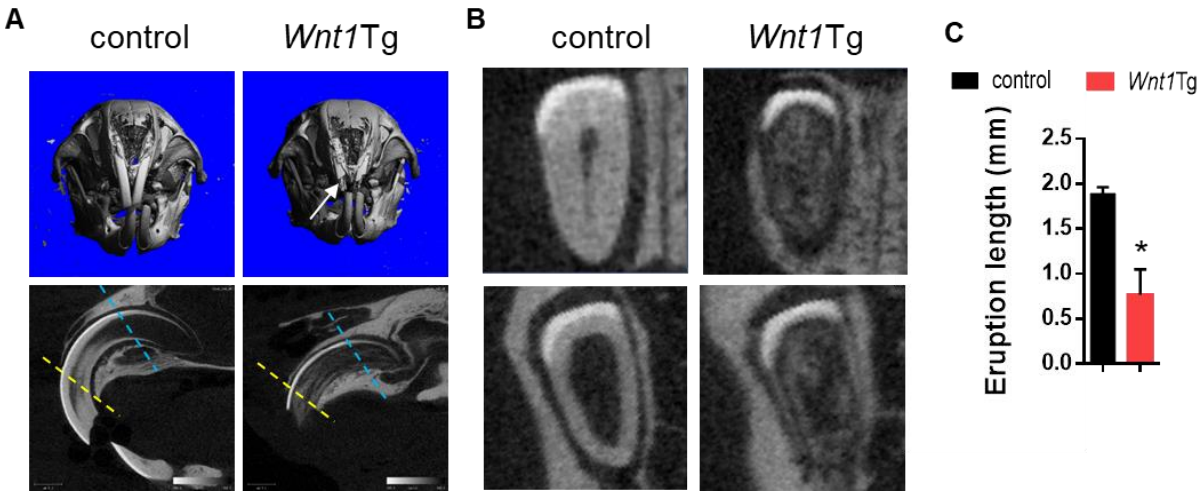

Figure 3.5 Wnt1 affects incisor formation in aged mice. A) µCT 3D-reconstructions of the skull (upper panels) and sagittal cross-sections of upper incisors (lower panels) from 1-year-old control and *Wnt1*-transgenic mice. Loss of enamel is present in *Wnt1*-trangenic mice (white arrow). Yellow and blue dashed lines indicate regions of the cross-sections shown in the upper and lower panels in B, respectively. B) Cross-sections of the maxillary incisors. Note that dentin formation is severely disturbed in *Wnt1*-transgenic mice. C) Quantification of the length of the erupted incisors in control and *Wnt1*-transgenic mice. n≥7. Data are the means ± SEM. **P* < 0.05.

3.2.3 Wnt1 overexpression affects maxillary molars and incisors in aged mice

In order to analyze and identify the teeth structures, paraffin histology of the decalcified maxillary first molar and the decalcified maxillary incisor was performed. The cellular cementum area was visualized in toluidine blue staining of the maxillary molars (Figure

3.6, A), and the acellular thickness was visualized in H&E stained sections of the maxillary incisors (Figure 3.6, B). The cellular cementum area and acellular thickness were analyzed by ImageJ toolbox, and they had a significant decrease in *Wnt1*-transgenic mice compared to control mice (Figure 3.6, C). However, compared to control mice, the structure of dentin and pulp did not have a significant change in *Wnt1*-transgenic mice (Figure 3.6, A.B). The toluidine blue sections of decalcified maxillary incisors clearly showed noticeable changes of the hard tissue structure in incisors. Compared to control mice, the dentin and pulp were replaced by loose calcified tissue in *Wnt1*-transgenic mice (Figure 3.6, D). The results indicate that Wnt1 has a downstream influence on cementum cells and interferes with growing teeth.

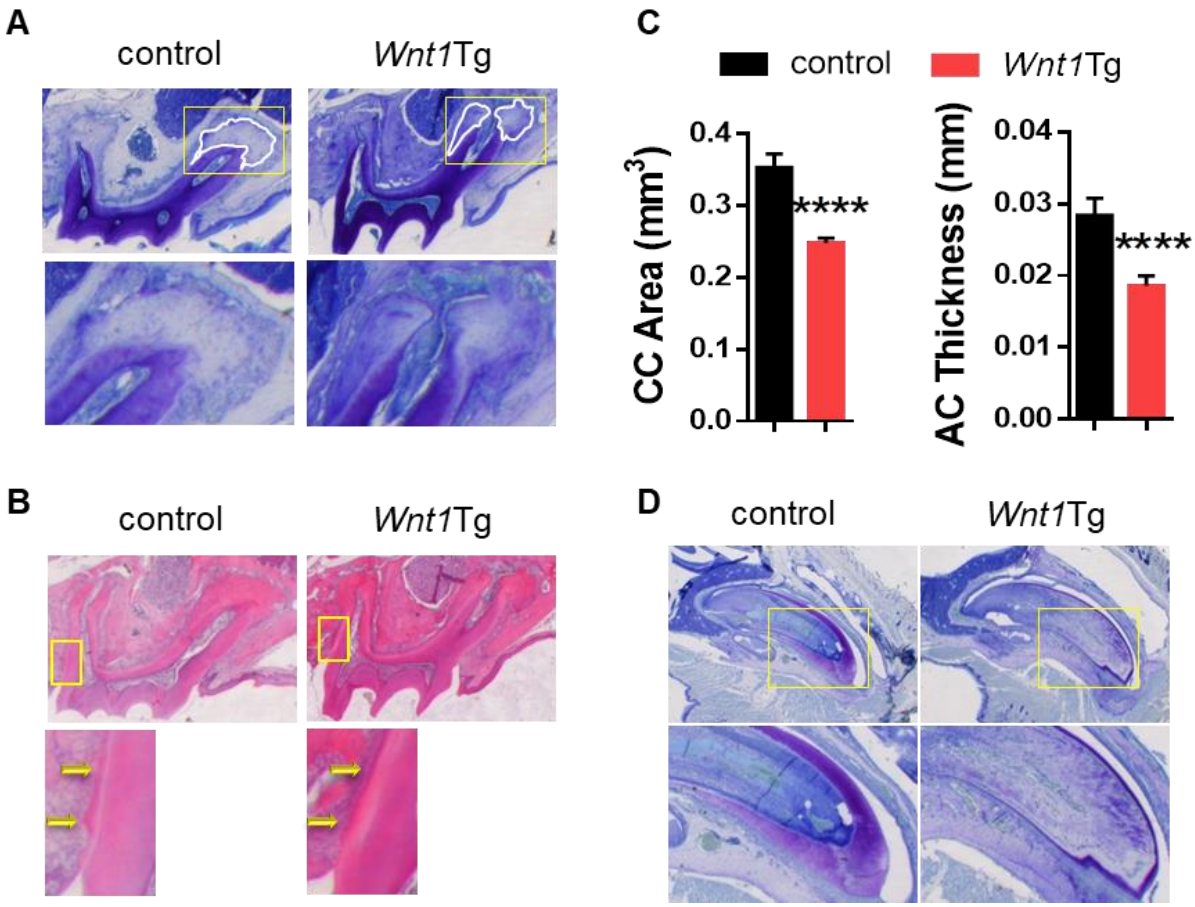

Figure 3.6 Wnt1 overexpression affects maxillary molars and incisors in aged mice. A) Toluidine blue stained sections of decalcified maxillary first molars of 1-year-old mice of the indicated genotype kept for 9 weeks under doxycycline-free food. The white lines indicate the cellular cementum measurement area. B) H&E stained sections of the decalcified maxillary first molars show details of the

acellular cementum. Yellow arrows show the acellular cementum. C) Quantification of cellular cementum (CC) and acellular cementum (AC). D) Toluidine blue stained sections of decalcified maxillary incisors show changing incisor structure in *Wnt1*-transgenic mice compared to control mice. n≥3 (C). Data are the means ± SEM. ****P < 0.0001.

3.3 Effect of Wnt1 over-expression on OCCM cementoblasts

3.3.1 Generation of cementoblasts stably over-expressing Wnt1

Since an analysis of 6-week-old animals, which was performed in our group, indicated increased cementoblast activity in *Wnt1*-transgenic mice, we hypothesized that the bone-like tissues inside the incisors of aged mice might be the consequence of cementoblast activation. Therefore, cell culture experiments using the OCCM cementoblast cell line were designed. These cells, which were originally isolated from the tooth root surface of OC-TAg mice that contain the SV40 large T-antigen (TAg) under control of the osteocalcin (OC) promoter and are capable of surviving serial passages in vitro. The immortalized cementoblasts obtained in this manner were subcloned, and one clone was designated as OCCM (D'Errico et al. (2000)). For the present project, stably transfected OCCM cells over-expressing Wnt1 were generated using an expression vector, where Wnt1 is fused to an HA-Tag (pLNCX-Wnt1) (Figure 3.7, A). OCCM cells were transfected with the plasmid using Lipofectamine at 70-90% confluency, incubated for 1-3 days, followed by selection with G418-BC. After 2-3 passages, OCCM cells were used for differentiation experiments (Figure 3.7, B). To confirm the success of the OCCM cell transfection and selection process, qRT-PCR was performed to measure the expression of Wnt1 compared with the empty vector transfection controls. Wnt1 over-expression in the first, second, and third transfection of the OCCM cells could be shown (Figure 3.7, C). Western blotting showed that Wnt1 is over-expressed in the 3 independent OCCM cell cultures transfected with the Wnt1 expression plasmid (Figure 3.7, D). Thus, OCCM cells could be successfully transfected with the Wnt1 plasmid. However, by Elisa using the media of vector transfection controls and the 3 independent Wnt1 over-expressing OCCM cell cultures, as well as the parental OCCM cell, no Wnt1 could be detected (Figure 3.7, E).

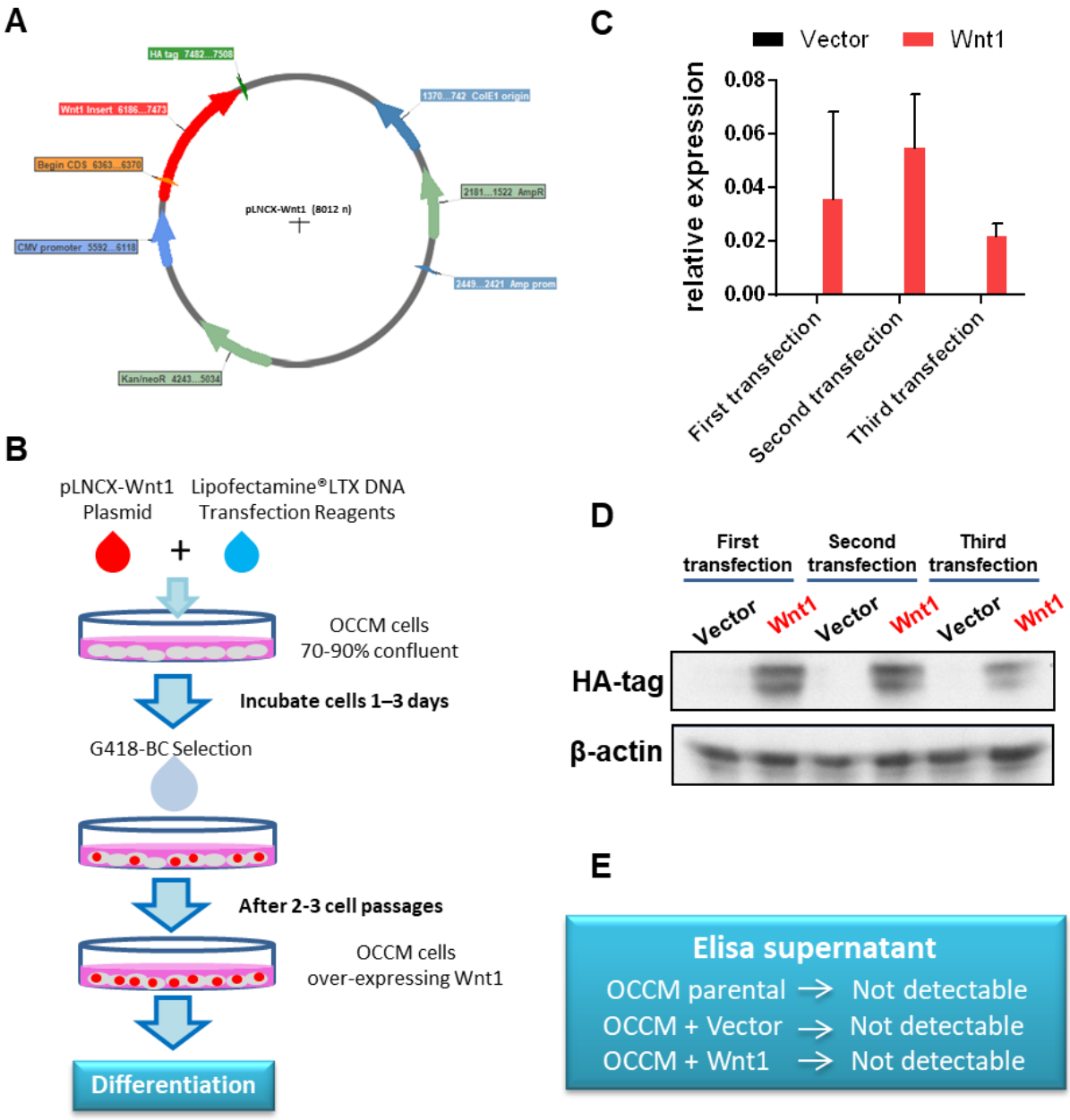

Figure 3.7 Generation of cementoblasts stably over-expressing Wnt1. A) Wnt1 HA-tag plasmid used for OCCM cell line transfection. B) Protocol for generating stably transfected OCCM cells over-expressing Wnt1. C) qRT-PCR quantification of the levels of mRNA encoding Wnt1 in 3 independently transfected OCCM cell lines. Wnt1 was not detected in the vector-transfected controls. D) Western blot analysis of Wnt1 expression using an HA-Tag antibody using protein extracts isolated from the 3 independently transfected OCCM cell cultures over-expressing Wnt1 compared to vector-transfected controls. E) Summary of Elisa detection of Wnt1 in the media of the 3 independent OCCM cell cultures over-expressing Wnt1 compared to vector-transfected controls. Data are the means ± SEM.

3.3.2 Wnt1 over-expression increases cell growth but has no effect on differentiation of OCCM cells

To analyze the influence of Wnt1 over-expression in OCCM cells, the cell number was counted daily in 3 independent Wnt1 over-expressing OCCM cells and vector-transfected controls. The results show that Wnt1 over-expression increases the numbers of OCCM cells (Figure 3.8, A). Subsequently the differentiation capacity of OCCM cells was checked by using Alizarin Red staining (Figure 3.8, B) and quantification of Alizarin Red incorporation (Figure 3.8, C). However, no significant difference between Wnt1 over-expressing OCCM cells and vector-transfected controls could be detected. Thus, the Wnt1 over-expression enhances cell growth, but not differentiation of OCCM cells.

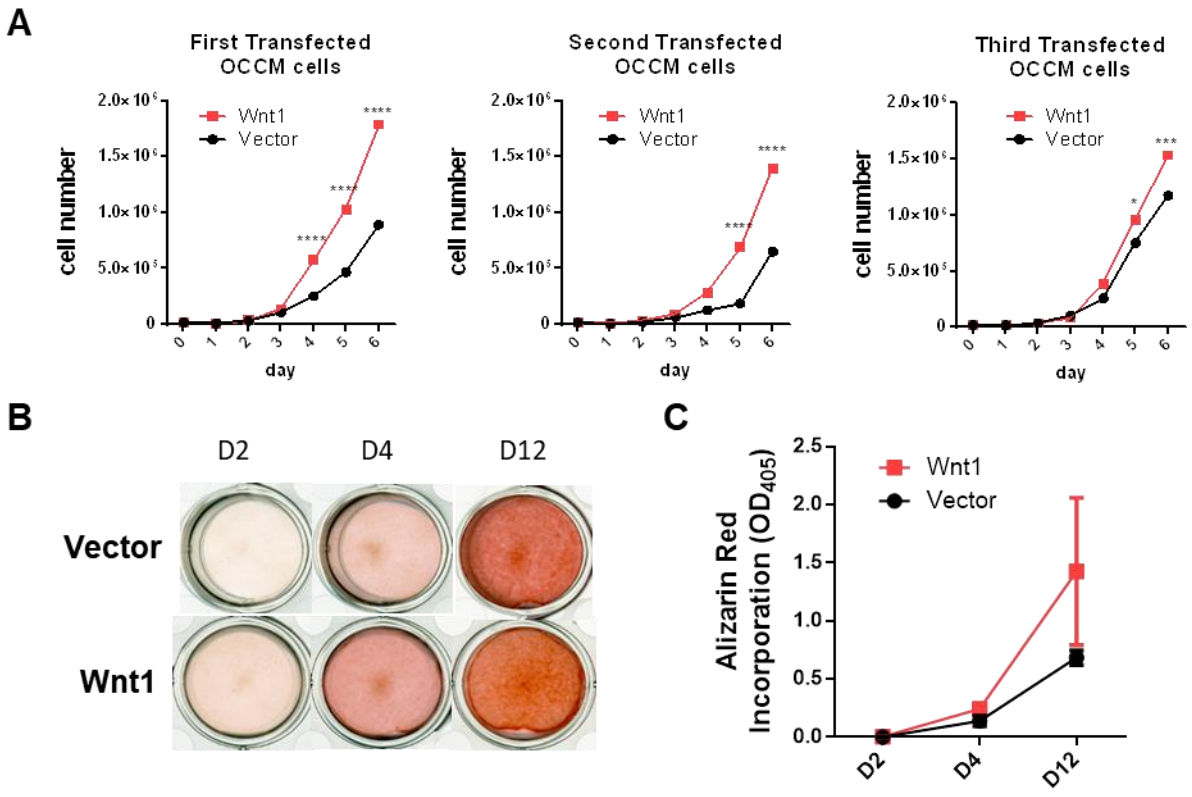

Figure 3.8 Wnt1 overexpression increases cell growth, but has no effect on the differentiation of OCCM cells. A) Increased cell growth in 3 independent Wnt1 over-expressing OCCM cell cultures compared to vector-transfected controls. B&C) Representative pictures of Alizarin Red staining (B) and quantification of Alizarin Red incorporation (C) of 3 independent *Wnt1*-overexpressing OCCM cell cultures compared to vector-transfected controls. Data are the means ± SEM. ****P < 0.0001; ***P < 0.001; *P < 0.05.

3.3.3 Transfection impairs of expression of mineralization-associated genes

To further understand the influence of Wnt1 on OCCM cells, we performed qRT-PCR. First, we checked expression of genes associated with bone mineralization, i.e. Bone sialoprotein 2 (*Ibsp*), Phosphate-regulating neutral endopeptidase (*Phex*), Osteopontin (*Spp1*), and Alkaline phosphatase (*Alpl*). Here we compared the OCCM cells over-expressing Wnt1 to OCCM cells transfected with empty vector and to non-transfected OCCM cells. For *Ibsp* and *Phex,* there was no significant difference among these three culture conditions (Figure 3.9, A.B). For *Spp1* and *Alpl*, Wnt1 over-expressing OCCM cells and empty vector OCCM cells expressed lower levels than the non-transfected OCCM cells (Figure 3.9, C.D). These results indicated that the transfection itself, either with Wnt1 or with empty vector, reduces the expression of mineralization-associated genes. Second, we also checked genes involved in cell proliferation, i.e. Fos-related antigen 1 (*Fosl1*) and Ankyrin 1 (*Ank1*). Again, at least in the case of Ank1 expression, there was a negative influence of the cell transfection, either with Wnt1 expression plasmids or with empty vector (Figure 3.9, E.F). Therefore, these experiments did not allow conclusions about the influence of Wnt1.

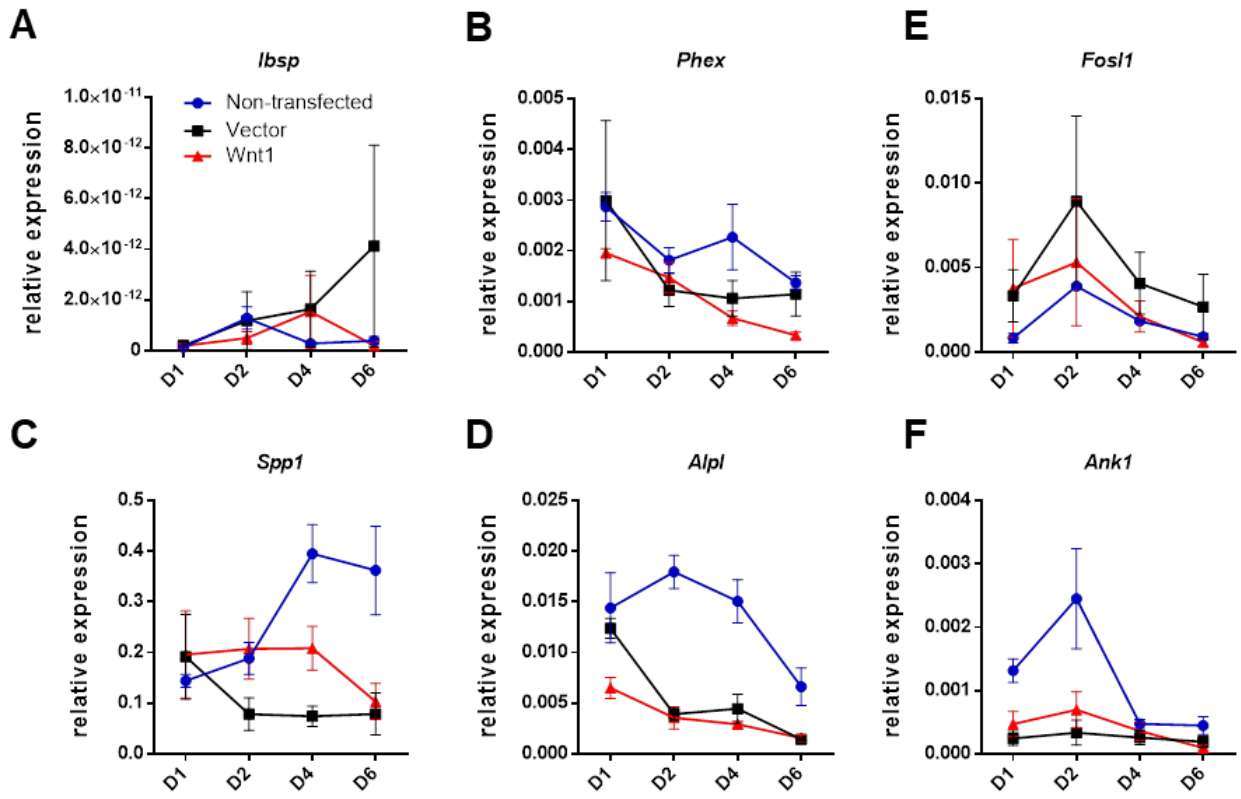

Figure 3.9 Transfection impairs of gene expression in OCCM cells. qRT-PCR quantification for expression of *Ibsp* (A), *Phex* (B), *Spp1* (C), *Alpl* (D), *Fosl1* (E), *Ank1* (F) in non-transfected OCCM cells, and OCCM cells transfected with the empty vector or the Wnt1 expression plasmid. Data are the means ± SEM.

3.3.4 Wnt1 over-expression induces Wnt signaling markers in OCCM cells

To analyze, which Wnt signaling pathway is induced by Wnt1 in OCCM cells, Western blotting and qRT-PCR were performed to check for specific pathway markers. The Western blotting results showed that Wnt1 over-expression induces active β-catenin (non-phosphorylated form), whereas there was no difference in the expression of β-catenin observed between empty vector and Wnt1 over-expressing OCCM cells. The expression of the phosphorylated S6 ribosomal protein was not affected by Wnt1 over-expression, suggesting that Wnt1 does not activate the S6 pathway. For cyclin D1, a downstream target of canonical Wnt signaling, our results showed a tendency of induction by Wnt1 (Figure 3.10, A). The activation of the canonical Wnt signaling pathway was principally confirmed by qRT-PCR, where a non-significantly increased

expression of *Axin2* and *Ccnd1* was observed (Figure 3.10, B). However, the other Wnt signaling pathway markers, i.e. β-catenin (*Ctnnb1*), *Lrp5, Lrp6, c-Myc, Apcdd1* and *Bglap* (Osteocalcin) were not found induced by Wnt1. Taken together, these data suggest that Wnt1 over-expression in OCCM cells may activate the canonical Wnt signaling pathway.

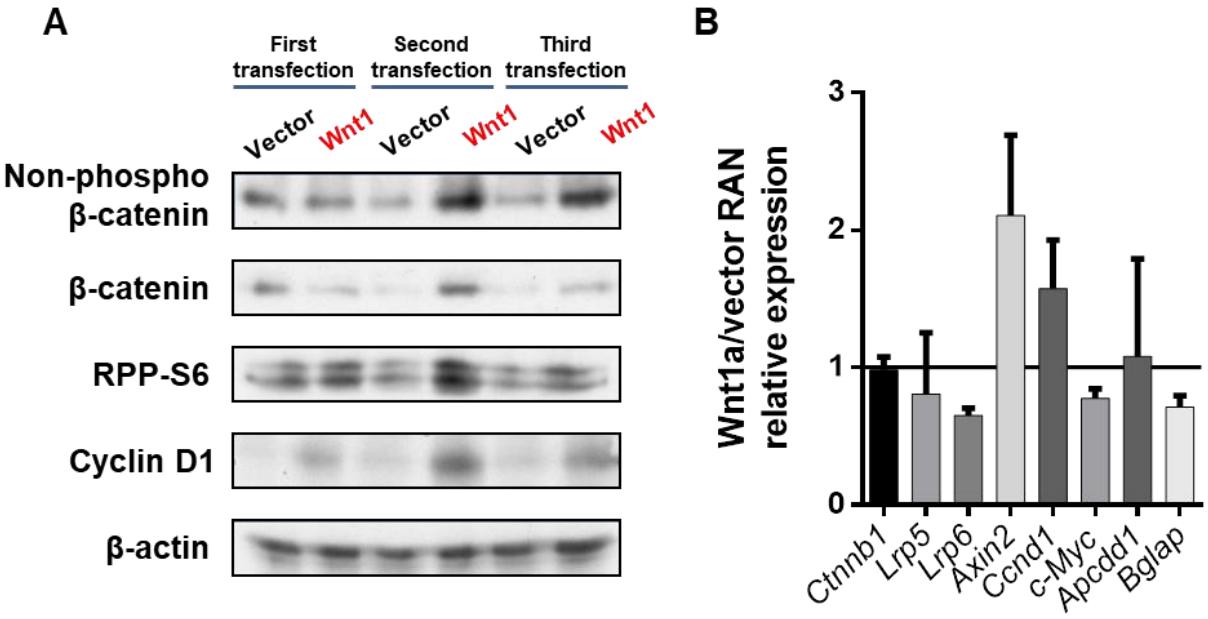

Figure 3.10 Wnt1 over-expression induces Wnt signaling markers. A) Western blot analysis of Wnt signaling pathway markers using antibodies against active β-catenin (non-phosphorylated form), total β-catenin, phosphorylated S6 ribosomal protein and Cyclin D1 in protein extracts isolated from 3 independently transfected OCCM cell cultures compared to vector-transfected controls. B) qRT-PCR quantification of mRNA levels encoding for β-catenin (*Ctnnb1*), *Lrp5*, *Lrp6*, *Axin2*, *Ccnd1*, *c-Myc*, *Apcdd1*, Osteocalcin (*Bglap*). Data are the means ± SEM.

4. Discussion

Osteoporosis is a chronic and progressive bone disease, in which the density and quality of bone is reduced, thereby increasing the risk of fractures. Osteoporosis usually has no symptoms until the first fracture occurs, which is the most common cause of additional fractures in the elderly. A very severe form of osteoporosis can also be found in children, where it is typically called osteogenesis imperfecta (OI). Recently, genetic technology has been widely used to clarify the cause of this disease. In 2013, Pyott et al. found the importance of WNT1 in the accrual and maintenance of bone mass by activating WNT signaling in osteoblasts (Pyott et al. (2013a)). This was the first time that a Wnt ligand was found to be linked to bone formation in humans.

Our group aims at understanding the mechanisms of Wnt1 to provide the basis for development of *Wnt1*-targeting drugs for the treatment of osteoporosis. Our data clearly showed that Wnt1 in growing mice significantly increased bone mass in trabecular and cortical bone. Moreover, when the tooth and alveolar bone were analyzed in growing *Wnt1*-overexpressing mice, it was found that Wnt1 causes ectopic bone formation, especially in the pulp cavity. However, as most patients with osteoporosis are elderly, the Wnt1 function in older mice still needed to be studied. This is why one-year-old mice were analyzed in this thesis.

It was found that Wnt1 functions also in old mice, since their trabecular and cortical bone mass were markedly increased by doxycycline removal. Further, the incisor and the molars were analyzed in 1-year-old mice. There were however no significant changes in alveolar bone and molars. In contrast, the incisor pulp chamber was filled by mineralized tissue, similar to what happens in the molar and incisor of growing mice. This suggested that Wnt1 has more influence on developing teeth.

Although the Wnt signaling pathway was found to play an important role during tooth development, the specific function of Wnt1 in this process is not fully clarified. Importantly however, Wnt1 was found to activate the canonical Wnt signaling pathway to increase β-catenin in dental pulp stem cells (DPSCs). B-catenin in turn inhibits odontoblasts differentiation to interfere with the mineralization process (Scheller et al. (2008)). This suggests that the mineralized tissue in the pulp chamber in aged *Wnt1*-tg

mice is not produced by odontoblasts. This is further confirmed by our previous work in Wnt1 over-expressing growing mice. Here we found, in undecalcified incisor sections stained with Masson-Golder trichrome, that the odontoblasts are normally aligned in *Wnt1*Tg mice without Wnt1 overexpression, but that no odontoblasts were found after 9 weeks of Wnt1 overexpression (Figure 4.1).

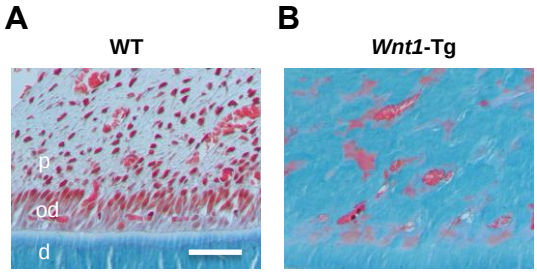

Figure 4.1 Wnt1 inhibits odontoblast differentiation. A) Undecalcified incisor sections of 6-week-old control mice (6 weeks DOX food) stained with Masson-Goldner trichrome. The pulp (p), odontoblasts (od) and dentin (d) layers are well organized. B) Undecalcified incisor sections of 12-week-old *Wnt1*-Tg mice (9 weeks DOX-free food) stained with Masson-Goldner trichrome. The clear stratified structure of pulp, odontoblasts and dentin disappeared. No odontoblasts can be found. Scale bar = 50 µm.

Because of these findings, the cementum was analyzed. The toluidine blue stained undecalcified tooth sections of 12-week-old control and *Wnt1*Tg overexpression mice showed that the acellular and cellular cementum are clearly thicker in *Wnt1*-Tg mice after 9 weeks of DOX removal. This was also confirmed by quantitative analysis (Figure 4.2). So we hypothesized that it is the cementum increasing in the pulp chamber, and that Wnt1 can induce cementoblasts. In order to confirm the influence of Wnt1 on cementoblats, cell culture experiments were designed. The cementoblast cell line OCCM was used, which express bone sialoprotein (BSP), osteopontin (OPN), and osteocalcin (OC) markers, and is widely used in the tooth development research. These cells also express type I and XII collagen and type I PTH/PTHrP receptor (D'Errico et al. (2000)).

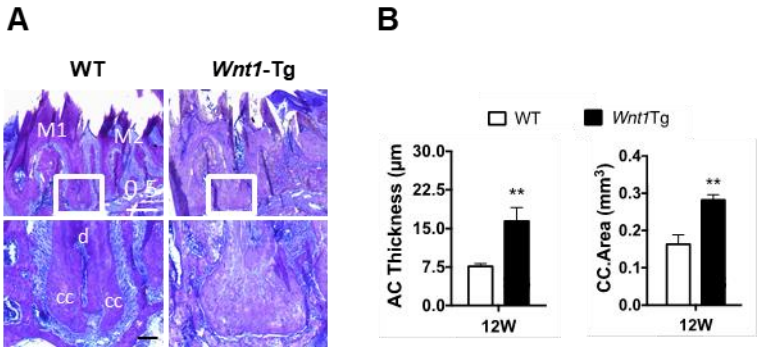

Figure 4.2 Wnt1 induces cementum differentiation. A) Toluidine staining of undecalcified molar sections of 6-week-old control mice (6 weeks DOX food) and *Wnt1*-Tg overexpression mice (9 weeks DOX-free food). The cementum (cc) area clearly increased in Wnt-overexpressing mice. (d = dentin) B) Quantification of acellar cementum thickness and cellar cementum area of control and *Wnt1*-Tg mice. Scale bar = 50 µm. n=3-5. Data are the means ± SEM. ***P* < 0.001.

The Wnt signaling pathway plays an important role in tooth root formation (Lohi et al. (2010)). Through the canonical Wnt pathway activation in molar root development, there is high expression of Axin2 and Wnt10a in root odontoblasts and preodontoblasts (Lohi et al. (2010); (Yamashiro et al. (2007)). Wnt3a is considered a crucial factor during tooth root formation (Nemoto et al. (2016)) and is recognized as a canonical Wnt ligand. There are three key proteins controlling Wnt ligand secretion – Porcupine, Wntless, and the retromer complex (Herr et al. (2012)). Wntless, discovered in 2006, is a multipass transmembrane protein (Ching and Nusse (2006)). It is thought to act as cargo receptor that ferries Wnt ligands along their exocytic path (Bänziger et al. (2006); Bartscherer et al. (2006); Goodman et al. (2006); Belenkaya et al. (2008); Franch-Marro et al. (2008); Port et al. (2008); Yang et al. (2008); MacDonald et al. (2009); Silhankova et al. (2010)). Wnt3a is recognized via Wntless to promote its secretion into the medium of producing cells. So Wnt3a conditioned media (CM) can be used to active canonical Wnt signaling. The Wnt1 secretion pathway is still under debate. Although overexpreSsed Porcn and Wls can significantly enhance the cell surface localization and secretion of Wnt1, this did not increase its biological activity (Galli et al. (2016)) (Figure 4.3). Since Wnt1 was not detected in the medium of cultured osteoblasts from *Wnt1*Tg mice, cell transfection was used to study the influence of Wnt1 on cementoblasts.

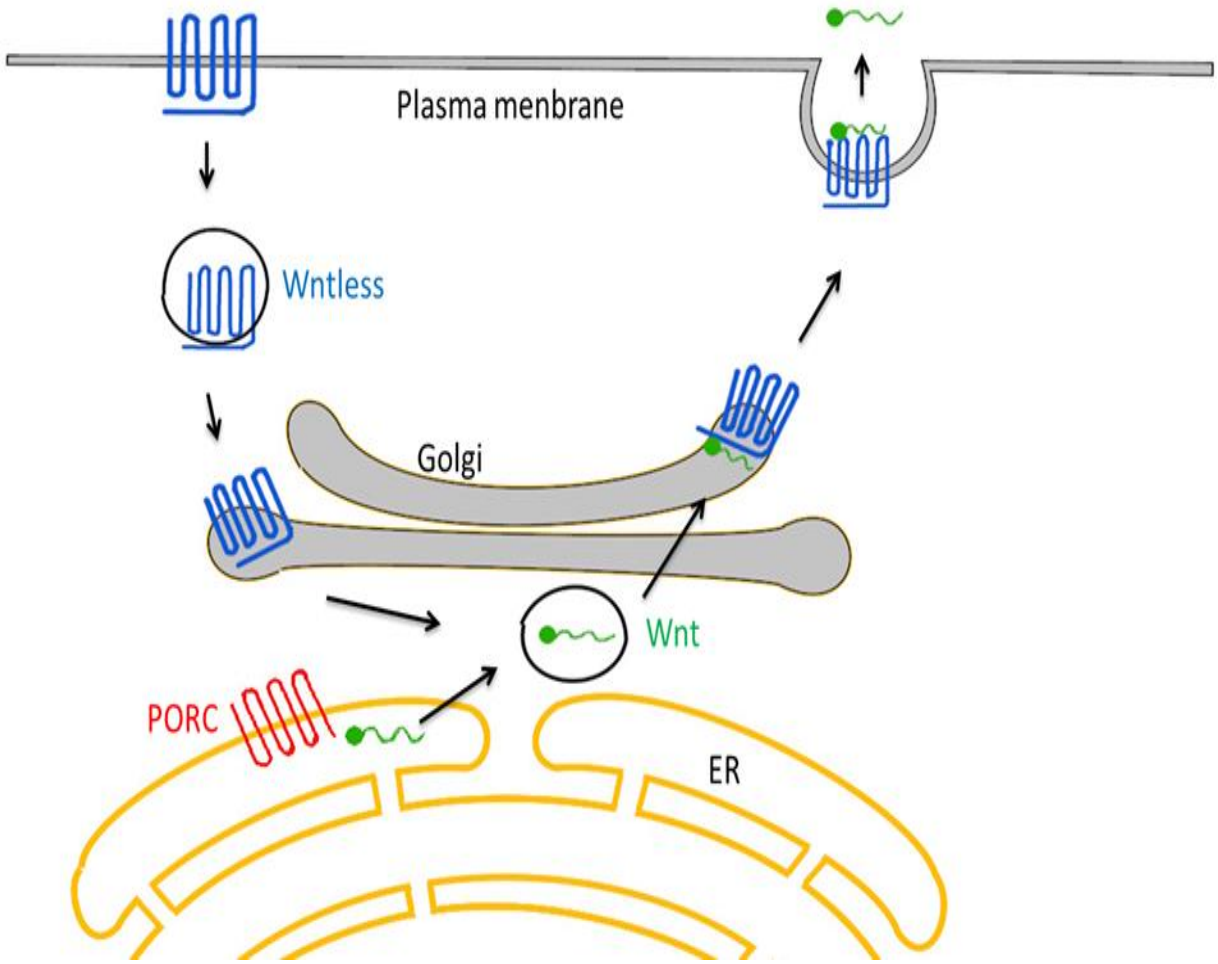

Figure 4.3 Schematic diagram of the Wnt secretion mechanism. The Wnt ligand becomes lipid-modified in the endoplasmic reticulum (ER) by the membrane-bound-O-acyltransferase porcupine (PORC). The lipidated Wnt is transported to the Golgi, binds to the Wntless multiple pass transmembrane protein, and escorts to the plasma membrane. Then the Wnt ligand is released into the extracellular space. The retromer complex is necessary for recycling of the Wntless endosomal vesicles.

Transfection is a process that introduces nucleic acids into eukaryotic cells (Transfection at the US National Library of Medicine Medical Subject Headings(MeSH)), and can result in unexpected morphologies and abnormalities in target cells. Generally, WNT-expressing OCCM cells were generated by transfection with the retroviral pLNCX vector expressing the specific WNT genes or LacZ gene under the control of the CMV promoter1 (Kispert et al. (1998); Arnold et al. (2000)). The Wnt1a pLNCX plasmid and

the pLNCX vector were separately transfected into the OCCM cells, to obtain Wnt1-expressing OCCM cells and vector OCCM cells controls. Antibiotic G418-BC was used to select transfected OCCM cells. G418-BC acts by binding the ribosome, thus inhibiting protein synthesis in both prokaryotic and eukaryotic cells. It thereby eliminates cells which did not integrate the plasmids containing a resistance gene. The success of transfection was confirmed by qRT-PCR and western blot. ELISA was performed to analyze the culture medium of Wnt1-expressing OCCM cells, but similar to the previous experiments, Wnt1 was not detected.

Importantly, Wnt1 notably increased the proliferation of OCCM cells, while it inhibited the differentiation of OCCM cells. These findings are in agreement with data by Nemoto et al, who used Lithium chloride (LiCl) and Wnt3a conditioned media (CM) to activate canonical Wnt signaling. These authors found that the Wnt signaling pathway inhibits cementoblasts differentiation, but enhances cell proliferation (Nemoto et al. (2009)). There was no significant difference in differentiation between the OCCM vector and Wnt1-expressing OCCM cells, but we found that the transfection itself reduces the expression of mineralization-associated genes. Therefore, we could not draw conclusions about the influence of Wnt1 on OCCM differentiation.

5. Summary

Wnt1 mutations lead to severe osteoporosis, suggesting a key role of Wnt1 in bone metabolism. We have previously shown that inducible osteoblast-specific over-expression of Wnt1 enhances bone formation in growing mice. The purpose of this study was to investigate the influence of Wnt1 on teeth in aged mice. It was found that Wnt1 induction in 52-week-old mice significantly increased trabecular and cortical bone mass. Moreover, these mice displayed mineralized tissue fillings in the incisor pulp chamber without significant changes in alveolar bone and molar. Finally, Wnt1 transfected OCCM cementoblasts were analyzed to determine the source of mineralized tissue in pulp chamber of the incisor. The quantification of Alizarin Red incorporation, qRT-PCR, and western blotting results confirmed that Wnt1 enhances proliferation of OCCM cells, while it inhibits their differentiation. Thus, we conclude that Wnt1 influences developing teeth by activating the canonical Wnt signaling pathway.

6. Zusammenfassung

Wnt1-Mutationen führen zu schwerer Osteoporose, was auf eine Schlüsselrolle von Wnt1 im Knochenstoffwechsel hindeutet. Wir haben bereits gezeigt, dass eine induzierbare osteoblastenspezifische Überexpression von Wnt1 die Knochenbildung in wachsenden Mäusen fördert. Der Zweck dieser Studie war es, den Einfluss von Wnt1 auf die Zähne bei gealterten Mäusen zu untersuchen. Es wurde festgestellt, dass die Wnt1-Induktion bei 52 Wochen alten Mäusen die trabekuläre und kortikale Knochenmasse signifikant erhöht. Darüber hinaus zeigten diese Mäuse mineralisierte Gewebefüllungen in der Pulpenkammer des Schneidezahns ohne signifikante Veränderungen des alveolären Knochens und der Molaren. Schließlich wurden Wnt1-transfizierte OCCM-Zementoblasten analysiert, um den Ursprung des mineralisierten Gewebes in der Pulpenkammer des Schneidezahns zu bestimmen. Die Quantifizierung der Alizarinrot-Inkorporation, qRT-PCR und Western-Blotting-Ergebnisse bestätigten, dass Wnt1 die Proliferation von OCCM-Zellen fördert, während die Differenzierung gehemmt wird. Daraus schließen wir, dass Wnt1 die Entwicklung der Zähne durch die Aktivierung des kanonischen Wnt-Signalwegs beeinflusst.

7. Abbreviations

µCT	Micro-computed tomography
2D	Two-dimensional
3D	Three-dimensional
ABC	Alveolar bone crest
Alpl	Alkaline phosphatase
Ank1	Ankyrin 1
BMP	Bone morphogenetic protein
BSP	Bone sialoprotein
CEJ	Cementum-enamel-junction
CK1	Casein kinase 1
CM	C conditioned media
DAAM1	Dishevelled-associated activator of morphogenesis 1
DKK	Dickkopf
DMEM	Dulbecco’s Modified Eagle Medium
DPSCs	Dental pulp stem cells
Dspp	Dentin sialophosphoprotein
DVL	Dishevelled
EDTA	Ethylenediaminetetraacetic acid
ELISA	Enzyme-linked immunosorbent assay

ER	Endoplasmic reticulum
et al.	et alii / aliae
EtOH	Alcohol Ethanol
FBS	Fetal Bovine Serum
FGFRs	FGF receptors
FGFs	Fibroblast Growth Factors
Fosl1	Fos-related antigen 1
Fzd	Frizzled
Gapdh	Glycerinaldehyde-3-phosphate-dehydrogenase
GSK-3β	Glycogen Synthase Kinase 3 Beta
H&E	Hematoxylin and eosin
hDPCs	Human dental papilla cells
HERS	Hertwig’s epithelial root sheath
Ibsp	Bone sialoprotein 2
IEE	Inner enamel epithelium
LiCl	Lithium chloride
LRP	Lipoprotein receptor-related proteins
MeSH	Medicine Medical Subject Headings
OC	Osteocalcin
OCCM	Cementum cell line osteocalcin promoter cementoblast

od	Odontoblasts
OI	Osteogenesis imperfecta
OPN	Osteopontin
Phex	Phosphate-regulating neutral endopeptidase
PORC	Membrane-bound-O-acyltransferase porcupine
qRT-PCR	Quantitative Real-Time PCR
RIPA	Radio-immunoprecipitation assay
SDS-PAGE	Sodium dodecyl sulfate–polyacrylamide gel electrophoresis
sFRP	Secreted frizzled related protein
Shh	Sonic hedgehog
SOST	Sclerostin
Spp1	Osteopontin
TCF/LEF	T-cell factor/lymphoid enhancer-binding factor
WIF-1	Wnt inhibitory factor-1
μm	Micro-meter

8. References

Ahn Y, Sanderson BW, Klein OD, Krumlauf R. 2010. Inhibition of wnt signaling by wise (sostdc1) and negative feedback from shh controls tooth number and patterning. Development. 137(19):3221-3231.

Aldinger KA, Mendelsohn NJ, Chung BH, Zhang W, Cohn DH, Fernandez B, Alkuraya FS, Dobyns WB, Curry CJ. 2016. Variable brain phenotype primarily affects the brainstem and cerebellum in patients with osteogenesis imperfecta caused by recessive wnt1 mutations. J Med Genet. 53(6):427-430.

Arce L, Yokoyama NN, Waterman ML. 2006. Diversity of lef/tcf action in development and disease. Oncogene. 25(57):7492-7504.

Arnold SJ, Stappert J, Bauer A, Kispert A, Herrmann BG, Kemler R. 2000. Brachyury is a target gene of the wnt/beta-catenin signaling pathway. Mechanisms of development. 91(1-2):249-258.

Bänziger C, Soldini D, Schütt C, Zipperlen P, Hausmann G, Basler K. 2006. Wntless, a conserved membrane protein dedicated to the secretion of wnt proteins from signaling cells. Cell. 125(3):509-522.

Bartscherer K, Pelte N, Ingelfinger D, Boutros M. 2006. Secretion of wnt ligands requires evi, a conserved transmembrane protein. Cell. 125(3):523-533.

Bei M, Maas R. 1998. Fgfs and bmp4 induce both msx1-independent and msx1-dependent signaling pathways in early tooth development. Development (Cambridge, England). 125(21):4325-4333.

Belenkaya TY, Wu Y, Tang X, Zhou B, Cheng L, Sharma YV, Yan D, Selva EM, Lin X. 2008. The retromer complex influences wnt secretion by recycling wntless from endosomes to the trans-golgi network. Developmental cell. 14(1):120-131.

Biggs LC, Mikkola ML. 2014. Early inductive events in ectodermal appendage morphogenesis. Seminars in cell & developmental biology. 25-26:11-21.

Bovolenta P, Esteve P, Ruiz JM, Cisneros E, Lopez-Rios J. 2008. Beyond wnt inhibition: New functions of secreted frizzled-related proteins in development and disease. J Cell Sci. 121(Pt 6):737-746.

Brunkow ME, Gardner JC, Van Ness J, Paeper BW, Kovacevich BR, Proll S, Skonier JE, Zhao L, Sabo P, Fu Y-H. 2001. Bone dysplasia sclerosteosis results from loss of

the sost gene product, a novel cystine knot–containing protein. The American Journal of Human Genetics. 68(3):577-589.

Ching W, Nusse R. 2006. A dedicated wnt secretion factor. Cell. 125(3):432-433.

Cho S-W, Kwak S, Woolley TE, Lee M-J, Kim E-J, Baker RE, Kim H-J, Shin J-S, Tickle C, Maini PK et al. 2011. Interactions between shh, sostdc1 and wnt signaling and a new feedback loop for spatial patterning of the teeth. Development (Cambridge, England). 138(9):1807-1816.

D'Errico JA, Berry JE, Ouyang H, Strayhorn CL, Windle JJ, Somerman MJ. 2000. Employing a transgenic animal model to obtain cementoblasts in vitro. J Periodontol. 71(1):63-72.

Dassule HR, McMahon AP. 1998. Analysis of epithelial–mesenchymal interactions in the initial morphogenesis of the mammalian tooth. Developmental biology. 202(2):215-227.

De Moerlooze L, Spencer-Dene B, Revest JM, Hajihosseini M, Rosewell I, Dickson C. 2000. An important role for the iiib isoform of fibroblast growth factor receptor 2 (fgfr2) in mesenchymal-epithelial signalling during mouse organogenesis. Development (Cambridge, England). 127(3):483-492.

Faqeih E, Shaheen R, Alkuraya FS. 2013. Wnt1 mutation with recessive osteogenesis imperfecta and profound neurological phenotype. J Med Genet. 50(7):491-492.

Fjeld K, Kettunen P, Furmanek T, Kvinnsland IH, Luukko K. 2005. Dynamic expression of wnt signaling-related dickkopf1, -2, and -3 mrnas in the developing mouse tooth. Developmental dynamics : an official publication of the American Association of Anatomists. 233(1):161-166.

Franch-Marro X, Wendler F, Guidato S, Griffith J, Baena-Lopez A, Itasaki N, Maurice MM, Vincent J-P. 2008. Wingless secretion requires endosome-to-golgi retrieval of wntless/evi/sprinter by the retromer complex. Nat Cell Biol. 10(2):170-177.

Galli LM, Zebarjadi N, Li L, Lingappa VR, Burrus LW. 2016. Divergent effects of porcupine and wntless on wnt1 trafficking, secretion, and signaling. Experimental cell research. 347(1):171-183.

Gong Y, Slee RB, Fukai N, Rawadi G, Roman-Roman S, Reginato AM, Wang H, Cundy T, Glorieux FH, Lev D et al. 2001. Ldl receptor-related protein 5 (lrp5) affects bone accrual and eye development. Cell. 107(4):513-523.

Goodman RM, Thombre S, Firtina Z, Gray D, Betts D, Roebuck J, Spana EP, Selva EM. 2006. Sprinter: A novel transmembrane protein required for wg secretion and signaling. Development (Cambridge, England). 133(24):4901-4911.

Gordon MD, Nusse R. 2006. Wnt signaling: Multiple pathways, multiple receptors, and multiple transcription factors. The Journal of biological chemistry. 281(32):22429-22433.

Gritli-Linde A, Bei M, Maas R, Zhang XM, Linde A, McMahon AP. 2002. Shh signaling within the dental epithelium is necessary for cell proliferation, growth and polarization. Development (Cambridge, England). 129(23):5323-5337.

He X, Semenov M, Tamai K, Zeng X. 2004. Ldl receptor-related proteins 5 and 6 in wnt/beta-catenin signaling: Arrows point the way. Development (Cambridge, England). 131(8):1663-1677.

Herr P, Hausmann G, Basler K. 2012. Wnt secretion and signalling in human disease. Trends in molecular medicine. 18(8):483-493.

Hjalt TA, Semina EV, Amendt BA, Murray JC. 2000. The pitx2 protein in mouse development. Developmental dynamics : an official publication of the American Association of Anatomists. 218(1):195-200.

Hosokawa R, Deng X, Takamori K, Xu X, Urata M, Bringas P, Jr., Chai Y. 2009. Epithelial-specific requirement of fgfr2 signaling during tooth and palate development. J Exp Zool B Mol Dev Evol. 312B(4):343-350.

Huang H, He X. 2008. Wnt/beta-catenin signaling: New (and old) players and new insights. Curr Opin Cell Biol. 20(2):119-125.

Hunter DJ, Bardet C, Mouraret S, Liu B, Singh G, Sadoine J, Dhamdhere G, Smith A, Tran XV, Joy A et al. 2015. Wnt acts as a prosurvival signal to enhance dentin regeneration. Journal of bone and mineral research : the official journal of the American Society for Bone and Mineral Research. 30(7):1150-1159.

Jernvall J, Aberg T, Kettunen P, Keranen S, Thesleff I. 1998. The life history of an embryonic signaling center: Bmp-4 induces p21 and is associated with apoptosis in the mouse tooth enamel knot. Development. 125(2):161-169.

Jernvall J, Thesleff I. 2000. Reiterative signaling and patterning during mammalian tooth morphogenesis. Mechanisms of development. 92(1):19-29.

Jheon AH, Seidel K, Biehs B, Klein OD. 2013. From molecules to mastication: The development and evolution of teeth. Wiley interdisciplinary reviews Developmental biology. 2(2):165-182.

Keränen SV, Kettunen P, Aberg T, Thesleff I, Jernvall J. 1999. Gene expression patterns associated with suppression of odontogenesis in mouse and vole diastema regions. Dev Genes Evol. 209(8):495-506.

Kettunen P, Laurikkala J, Itäranta P, Vainio S, Itoh N, Thesleff I. 2000. Associations of fgf-3 and fgf-10 with signaling networks regulating tooth morphogenesis. Developmental dynamics : an official publication of the American Association of Anatomists. 219(3):322-332.

Kettunen P, Thesleff I. 1998. Expression and function of fgfs-4, -8, and -9 suggest functional redundancy and repetitive use as epithelial signals during tooth morphogenesis. Developmental dynamics : an official publication of the American Association of Anatomists. 211(3):256-268.

Keupp K, Beleggia F, Kayserili H, Barnes AM, Steiner M, Semler O, Fischer B, Yigit G, Janda CY, Becker J et al. 2013. Mutations in wnt1 cause different forms of bone fragility. American journal of human genetics. 92(4):565-574.

Kimelman D, Xu W. 2006. Beta-catenin destruction complex: Insights and questions from a structural perspective. Oncogene. 25(57):7482-7491.

Kispert A, Vainio S, McMahon AP. 1998. Wnt-4 is a mesenchymal signal for epithelial transformation of metanephric mesenchyme in the developing kidney. Development (Cambridge, England). 125(21):4225-4234.

Klein OD, Minowada G, Peterkova R, Kangas A, Yu BD, Lesot H, Peterka M, Jernvall J, Martin GR. 2006. Sprouty genes control diastema tooth development via bidirectional antagonism of epithelial-mesenchymal fgf signaling. Developmental cell. 11(2):181-190.

Kratochwil K, Dull M, Farinas I, Galceran J, Grosschedl R. 1996. Lef1 expression is activated by bmp-4 and regulates inductive tissue interactions in tooth and hair development. Genes & development. 10(11):1382-1394.

Kratochwil K, Galceran J, Tontsch S, Roth W, Grosschedl R. 2002. Fgf4, a direct target of lef1 and wnt signaling, can rescue the arrest of tooth organogenesis in lef1(-/-) mice. Genes & development. 16(24):3173-3185.

Kyrylkova K, Kyryachenko S, Biehs B, Klein O, Kioussi C, Leid M. 2012. Bcl11b regulates epithelial proliferation and asymmetric development of the mouse mandibular incisor. PloS one. 7(5):e37670-e37670.

Laine CM, Joeng KS, Campeau PM, Kiviranta R, Tarkkonen K, Grover M, Lu JT, Pekkinen M, Wessman M, Heino TJ et al. 2013. Wnt1 mutations in early-onset osteoporosis and osteogenesis imperfecta. N Engl J Med. 368(19):1809-1816.

Li J, Chatzeli L, Panousopoulou E, Tucker AS, Green JBA. 2016. Epithelial stratification and placode invagination are separable functions in early morphogenesis of the molar tooth. Development (Cambridge, England). 143(4):670-681.

Lin M, Li L, Liu C, Liu H, He F, Yan F, Zhang Y, Chen Y. 2011. Wnt5a regulates growth, patterning, and odontoblast differentiation of developing mouse tooth. Developmental dynamics : an official publication of the American Association of Anatomists. 240(2):432-440.

Lintern KB, Guidato S, Rowe A, Saldanha JW, Itasaki N. 2009. Characterization of wise protein and its molecular mechanism to interact with both wnt and bmp signals. The Journal of biological chemistry. 284(34):23159-23168.

Liu F, Chu EY, Watt B, Zhang Y, Gallant NM, Andl T, Yang SH, Lu MM, Piccolo S, Schmidt-Ullrich R et al. 2008. Wnt/beta-catenin signaling directs multiple stages of tooth morphogenesis. Developmental biology. 313(1):210-224.

Liu Y, Song L, Ma D, Lv F, Xu X, Wang J, Xia W, Jiang Y, Wang O, Song Y et al. 2016. Genotype-phenotype analysis of a rare type of osteogenesis imperfecta in four chinese families with wnt1 mutations. Clin Chim Acta. 461:172-180.

Logan CY, Nusse R. 2004. The wnt signaling pathway in development and disease. Annual review of cell and developmental biology. 20:781-810.

Lohi M, Tucker AS, Sharpe PT. 2010. Expression of axin2 indicates a role for canonical wnt signaling in development of the crown and root during pre- and postnatal tooth development. Developmental dynamics : an official publication of the American Association of Anatomists. 239(1):160-167.

Luckett WP. 1985. Superordinal and intraordinal affinities of rodents: Developmental evidence from the dentition and placentation. Evolutionary relationships among rodents. Springer. p. 227-276.

Luther J, Yorgan TA, Rolvien T, Ulsamer L, Koehne T, Liao N, Keller D, Vollersen N, Teufel S, Neven M. 2018. Wnt1 is an lrp5-independent bone-anabolic wnt ligand. Science translational medicine. 10(466):eaau7137.

Maas R, Bei M. 1997. The genetic control of early tooth development. Critical Reviews in Oral Biology & Medicine. 8(1):4-39.

MacDonald BT, Tamai K, He X. 2009. Wnt/beta-catenin signaling: Components, mechanisms, and diseases. Developmental cell. 17(1):9-26.

Mikels A, Minami Y, Nusse R. 2009. Ror2 receptor requires tyrosine kinase activity to mediate wnt5a signaling. The Journal of biological chemistry. 284(44):30167-30176.

Murashima-Suginami A, Takahashi K, Sakata T, Tsukamoto H, Sugai M, Yanagita M, Shimizu A, Sakurai T, Slavkin HC, Bessho K. 2008. Enhanced bmp signaling results in supernumerary tooth formation in usag-1 deficient mouse. Biochemical and biophysical research communications. 369(4):1012-1016.

Nakamura T, Nakamura T, Matsumoto K. 2008. The functions and possible significance of kremen as the gatekeeper of wnt signalling in development and pathology. J Cell Mol Med. 12(2):391-408.

Nemoto E, Koshikawa Y, Kanaya S, Tsuchiya M, Tamura M, Somerman MJ, Shimauchi H. 2009. Wnt signaling inhibits cementoblast differentiation and promotes proliferation. Bone. 44(5):805-812.

Nemoto E, Sakisaka Y, Tsuchiya M, Tamura M, Nakamura T, Kanaya S, Shimonishi M, Shimauchi H. 2016. Wnt3a signaling induces murine dental follicle cells to differentiate into cementoblastic/osteoblastic cells via an osterix-dependent pathway. Journal of periodontal research. 51(2):164-174.

Neubüser A, Peters H, Balling R, Martin GR. 1997. Antagonistic interactions between fgf and bmp signaling pathways: A mechanism for positioning the sites of tooth formation. Cell. 90(2):247-255.

Nie J, Sage EH. 2009. Sparc functions as an inhibitor of adipogenesis. Journal of cell communication and signaling. 3(3-4):247.

Nusse R, Varmus HE. 1982. Many tumors induced by the mouse mammary tumor virus contain a provirus integrated in the same region of the host genome. Cell. 31(1):99-109.

Nüsslein-Volhard C, Lohs-Schardin M, Sander K, Cremer C. 1980. A dorso-ventral shift of embryonic primordia in a new maternal-effect mutant of drosophila. Nature. 283(5746):474-476.

Peng L, Ren LB, Dong G, Wang CL, Xu P, Ye L, Zhou XD. 2010. Wnt5a promotes differentiation of human dental papilla cells. International endodontic journal. 43(5):404-412.

Peterková R, Peterka M, Vonesch JL, Ruch JV. 1995. Contribution of 3-d computer-assisted reconstructions to the study of the initial steps of mouse odontogenesis. Int J Dev Biol. 39(1):239-247.

Pispa J, Thesleff I. 2003. Mechanisms of ectodermal organogenesis. Developmental biology. 262(2):195-205.

Porntaveetus T, Otsuka-Tanaka Y, Basson MA, Moon AM, Sharpe PT, Ohazama A. 2011. Expression of fibroblast growth factors (fgfs) in murine tooth development. Journal of anatomy. 218(5):534-543.

Port F, Kuster M, Herr P, Furger E, Bänziger C, Hausmann G, Basler K. 2008. Wingless secretion promotes and requires retromer-dependent cycling of wntless. Nat Cell Biol. 10(2):178-185.

Prochazka J, Prochazkova M, Du W, Spoutil F, Tureckova J, Hoch R, Shimogori T, Sedlacek R, Rubenstein JL, Wittmann T et al. 2015. Migration of founder epithelial cells drives proper molar tooth positioning and morphogenesis. Developmental cell. 35(6):713-724.

Pummila M, Fliniaux I, Jaatinen R, James MJ, Laurikkala J, Schneider P, Thesleff I, Mikkola ML. 2007. Ectodysplasin has a dual role in ectodermal organogenesis: Inhibition of bmp activity and induction of shh expression. Development (Cambridge, England). 134(1):117-125.

Pyott SM, Tran TT, Leistritz DF, Pepin MG, Mendelsohn NJ, Temme RT, Fernandez BA, Elsayed SM, Elsobky E, Verma I. 2013a. Wnt1 mutations in families affected by moderately severe and progressive recessive osteogenesis imperfecta. The American Journal of Human Genetics. 92(4):590-597.

Pyott SM, Tran TT, Leistritz DF, Pepin MG, Mendelsohn NJ, Temme RT, Fernandez BA, Elsayed SM, Elsobky E, Verma I et al. 2013b. Wnt1 mutations in families affected

by moderately severe and progressive recessive osteogenesis imperfecta. American journal of human genetics. 92(4):590-597.

Rijsewijk F, Schuermann M, Wagenaar E, Parren P, Weigel D, Nusse R. 1987. The drosophila homolog of the mouse mammary oncogene int-1 is identical to the segment polarity gene wingless. Cell. 50(4):649-657.

Sakisaka Y, Tsuchiya M, Nakamura T, Tamura M, Shimauchi H, Nemoto E. 2015. Wnt5a attenuates wnt3a-induced alkaline phosphatase expression in dental follicle cells. Experimental cell research. 336(1):85-93.

Sarkar L, Cobourne M, Naylor S, Smalley M, Dale T, Sharpe PT. 2000. Wnt/shh interactions regulate ectodermal boundary formation during mammalian tooth development. Proc Natl Acad Sci U S A. 97(9):4520-4524.

Sarkar L, Sharpe PT. 1999. Expression of wnt signalling pathway genes during tooth development. Mechanisms of development. 85(1-2):197-200.

Scheller EL, Chang J, Wang CY. 2008. Wnt/beta-catenin inhibits dental pulp stem cell differentiation. Journal of dental research. 87(2):126-130.

Schlessinger K, Hall A, Tolwinski N. 2009. Wnt signaling pathways meet rho gtpases. Genes & development. 23(3):265-277.

Schour I, Massler M. 1940. Studies in tooth development: The growth pattern of human teeth part ii. The Journal of the American Dental Association. 27(12):1918-1931.

Silhankova M, Port F, Harterink M, Basler K, Korswagen HC. 2010. Wnt signalling requires mtm-6 and mtm-9 myotubularin lipid-phosphatase function in wnt-producing cells. EMBO J. 29(24):4094-4105.

St Amand TR, Zhang Y, Semina EV, Zhao X, Hu Y, Nguyen L, Murray JC, Chen Y. 2000. Antagonistic signals between bmp4 and fgf8 define the expression of pitx1 and pitx2 in mouse tooth-forming anlage. Developmental biology. 217(2):323-332.

Stephen J, Girisha KM, Dalal A, Shukla A, Shah H, Srivastava P, Kornak U, Phadke SR. 2015. Mutations in patients with osteogenesis imperfecta from consanguineous indian families. Eur J Med Genet. 58(1):21-27.

Takamori K, Hosokawa R, Xu X, Deng X, Bringas P, Jr., Chai Y. 2008. Epithelial fibroblast growth factor receptor 1 regulates enamel formation. Journal of dental research. 87(3):238-243.

Thesleff I. 2014. Current understanding of the process of tooth formation: Transfer from the laboratory to the clinic. Australian dental journal. 59 Suppl 1:48-54.

Thesleff I, Sharpe P. 1997. Signalling networks regulating dental development. Mechanisms of development. 67(2):111-123.

Toomes C, Bottomley HM, Jackson RM, Towns KV, Scott S, Mackey DA, Craig JE, Jiang L, Yang Z, Trembath R. 2004. Mutations in lrp5 or fzd4 underlie the common familial exudative vitreoretinopathy locus on chromosome 11q. The American Journal of Human Genetics. 74(4):721-730.

Tucker AS, Yamada G, Grigoriou M, Pachnis V, Sharpe PT. 1999. Fgf-8 determines rostral-caudal polarity in the first branchial arch. Development (Cambridge, England). 126(1):51-61.

Vaahtokari A, Aberg T, Thesleff I. 1996. Apoptosis in the developing tooth: Association with an embryonic signaling center and suppression by egf and fgf-4. Development. 122(1):121-129.

Vainio S, Karavanova I, Jowett A, Thesleff I. 1993. Identification of bmp-4 as a signal mediating secondary induction between epithelial and mesenchymal tissues during early tooth development. Cell. 75(1):45-58.

van Amerongen R, Nusse R. 2009. Towards an integrated view of wnt signaling in development. Development (Cambridge, England). 136(19):3205-3214.

van Genderen C, Okamura RM, Fariñas I, Quo RG, Parslow TG, Bruhn L, Grosschedl R. 1994. Development of several organs that require inductive epithelial-mesenchymal interactions is impaired in lef-1-deficient mice. Genes & development. 8(22):2691-2703.

Wang B, Li H, Liu Y, Lin X, Lin Y, Wang Y, Hu X, Zhang Y. 2014. Expression patterns of wnt/β-catenin signaling molecules during human tooth development. Journal of molecular histology. 45(5):487-496.

Yamashiro T, Zheng L, Shitaku Y, Saito M, Tsubakimoto T, Takada K, Takano-Yamamoto T, Thesleff I. 2007. Wnt10a regulates dentin sialophosphoprotein mrna expression and possibly links odontoblast differentiation and tooth morphogenesis. Differentiation; research in biological diversity. 75(5):452-462.

Yang P-T, Lorenowicz MJ, Silhankova M, Coudreuse DYM, Betist MC, Korswagen HC. 2008. Wnt signaling requires retromer-dependent recycling of mig-14/wntless in wnt-producing cells. Developmental cell. 14(1):140-147.

Yokohama-Tamaki T, Ohshima H, Fujiwara N, Takada Y, Ichimori Y, Wakisaka S, Ohuchi H, Harada H. 2006. Cessation of fgf10 signaling, resulting in a defective dental epithelial stem cell compartment, leads to the transition from crown to root formation. Development. 133(7):1359-1366.

9. Acknowledgements

Finally, I would like to express my thanks at this point. It applies to all those who accompanied, supported and animated me in this work:

First, I would like to thank my supervisor Dr. Jean-Pierre David, who warmly welcomed me to join the working group and led me step by step into the field of scientific research.

I want to thank PD Dr. Dr. Till Köhne for giving me such a precious opportunity to enable me to start my scientific studies on such a great experimental platform of the IOBM and give me the necessary guidance.

I am grateful to Prof. Dr. Thorsten Schinke for all his contributions to my scientific studies, including corrections of the dissertation.

I also thank Julia and Max for their great support in laboratory technical and university issues.

A big “thank you” to the entire IOBM team, above all Anke, Gretl, Lana, Mona, Nele, Olga, and Timur for the great support and help, patience, good advice, nice and funny talks and the relaxed, productive atmosphere.

Finally, of course, I would also like to thank my family for the constant support.

Thanks a lot!

10. Publication

Luther J, Yorgan TA, Rolvien T, Ulsamer L, Koehne T, **Liao N**, Keller D, Vollersen N, Teufel S, Neven M. 2018. Wnt1 is an lrp5-independent bone-anabolic wnt ligand. Science translational medicine. 10(466):eaau7137.

11. Lebenslauf

Lebenslauf wurde aus datenschutzrechtlichen Gründen entfernt

12. Eidesstattliche Versicherung

Ich versichere ausdrücklich, dass ich die Arbeit selbständig und ohne fremde Hilfe verfasst, andere als die von mir angegebenen Quellen und Hilfsmittel nicht benutzt und die aus den benutzten Werken wörtlich oder inhaltlich entnommenen Stellen einzeln nach Ausgabe (Auflage und Jahr des Erscheinens), Band und Seite des benutzten Werkes kenntlich gemacht habe.

Ferner versichere ich, dass ich die Dissertation bisher nicht einem Fachvertreter an einer anderen Hochschule zur Überprüfung vorgelegt oder mich anderweitig um Zulassung zur Promotion beworben habe.

Ich erkläre mich einverstanden, dass meine Dissertation vom Dekanat der Medizinischen Fakultät mit einer gängigen Software zur Erkennung von Plagiaten überprüft werden kann.

Unterschrift: .....